Cellulose Nanomaterial-based Films for Grease-resistance Food Packaging Application

by

Summia Rahman

A thesis submitted to the Graduate Faculty of
Auburn University
in partial fulfillment of the
requirements for the Degree of
Master of Science

Auburn, Alabama
August 5, 2023

Keywords: Cellulose nanofibrils, Grease resistance, Sustainable, Cellulose nanocrystals Polyethylene oxide, Food packaging

Approved by

Dr. Yucheng Peng, Chair, Assistant Professor of Forestry, Wildlife, and Environment,
Dr. Brian Via, committee member, Professor of Forestry, Wildlife, and Environment,
Dr. María Soledad Peresin, committee member, Associate Professor of Forestry, Wildlife, and Environment
Dr. Tom Gallagher, committee member, Professor of Forestry, Wildlife, and Environment

Abstract

The common uses of plastic for food packaging are advantageous in many cases because of its easy processability, low cost, and excellent resistance to water, oil, and grease penetration. The per- and poly-fluoroalkyl substances (PFASs) treated paper using the conventional paper manufacturing process has also achieved similar functionalities to prevent oil, water, and grease passages. However, due to the health and environmental concerns of the two packaging systems mentioned above, food packaging industries are now open to more options. A sustainable and health-promoting paper-based food packaging system that can restrict oil, water, and grease from passing through is highly desirable to fulfill the increasing demand for convenience food products. Cellulose nanomaterials (CNs), such as cellulose nanofibrils (CNFs) and cellulose nanocrystals (CNCs), are ideal alternatives. CNFs have excellent mechanical strength and gas barrier properties, but they have high hydrophilicity because of their amorphous structure and surface hydroxyl groups which decrease their properties whenever in contact with moisture or high humidity. On the other hand, CNCs are less chemically reactive to water due to their crystalline structure, but films prepared with only CNCs are very brittle. To overcome the limitations of each of these two CNs, this research studied films prepared by blending CNF and CNC suspensions at various ratios. Water-soluble polymer polyethylene oxide (PEO), widely known for coating applications, was added to the film formulation development process to optimize the film performance. This research aims to prepare standalone grease resistance films and/or coating materials for food packaging applications. The properties of the films were characterized by mechanical property tests, contact angle analysis, atomic force microscopy analysis, grease resistance test, pore size distribution

measurement, and Fourier-transform infrared spectroscopy (FTIR) analysis. Films prepared with 100% CNF showed better tensile strength (103 ± 11 MPa), strain at break (13% ± 0.02), and tensile energy absorption (9059.8 ± 2076.8 J/m^3) than all the other CNF/CNC composite films as well as commercially available parchment paper, butcher paper, pan liner, and copy paper. FTIR analysis reported that intermolecular hydrogen bonds of cellulose molecules were replaced by the hydrogen bonds between PEO and CNF in the films prepared with CNF/PEO. In addition, pore size distribution results reported that PEO helped reduce the overall pore size distribution of CNF film, which can be advantageous in grease resistance.

Acknowledgements

First, I would like to express my sincere gratitude to my mentor and advisor, Dr.Yucheng Peng, for his insightful advice, understanding, and support. His conscientious dedication and unwavering enthusiasm for science and research are inspiring. I am grateful to him for allowing me to learn and grow professionally throughout my MS program. His generous guidance and persistent help have significantly contributed to making this thesis writing possible. I sincerely acknowledge all my committee members, Drs. Brian Via, María Soledad Peresin, and Tom Gallagher, for their constant support, motivation, valuable input, and scientific discussions.

I would like to extend my gratitude to Dr. Zhihua Jiang, Auburn University, for always being very helpful and allowing me to use the Capillary flow porometer in his laboratory. I am also grateful to Dr. Ramsis Farag for teaching me how to test my samples' pore size and analyze the data. I sincerely thank Dr. María Soledad Peresin for allowing me to use dynamic light scattering (DLS) in her laboratory. I am grateful to you more than you know for always being supportive and kind-hearted in my Auburn journey. I want to thank Javier Hernandez for guiding me during DLS testing. I also want to thank Dr. Shaoyang Liu at Troy University for conducting the atomic force microscopy study for my film samples. Furthermore, I would like to express my sincere gratitude to Dr. Brian Via for always being supportive and allowing me to use Fourier-transform infrared spectroscopy with attenuated total reflection (FTIR-ATR) in his lab. I also would like to thank Dr. Beatriz Vega for her constant support during FTIR-ATR testing. I am very much thankful to Dr. George Flower, Dr. Maria Witte, and Dr. Dale Watson for making my Auburn journey incredibly beautiful. The amount of love, support, and care they showed me during the regional Three Minute

Thesis (3MT) competition in North Carolina was unparallel. I'm also very grateful to my friend Dr. Salman Baig for his phenomenal support in my academic career.

I want to thank my amazing lab mates Ke Zhang and Xuqi Wang for always being very helpful and awesome. Besides, I am very thankful for my wonderful Auburn friends: Anna, Abby, Yufei, Sydney, Shaun, Lauren, Molly, Katelyn, Muztahid, and Hannah, for always being there for me when I needed them. Thank you all for your amazing friendship.

Finally, I want to express my best gratitude and dedicate this thesis to my lovely parents. I can never thank you enough for all your unconditional love and support in achieving my goals. I want to thank my elder sister Samanta and younger brothers Sakib, and Sazid for always being a piece of happiness in my life and helping me to move forward.

Table of contents

Abstract ii

Acknowledgements iv

Table of content vi

List of tables ix

List of figures x

1. Literature Review 1

    1.1. Introduction 1

    1.2. Mechanisms of grease resistance for paper products 3

    1.3. New strategies to develop grease-resistant paper products 8

2. Problem statement and significance of the study 10

3. Materials and methods 12

    3.1 Raw material 12

    3.2. Particle size distribution 13

    3.3. Standalone CNF/CNC composite films 13

    3.4. Standalone CNF/PEO composite films 14

3.5. Characterization of films: 15

3.5.1. Mechanical properties 15

3.5.2. Contact angle measurement 16

3.5.4. Atomic Force Microscopy (AFM) 16

3.5.6. Fourier-transform infrared spectroscopy with attenuated total reflection (FTIR-ATR) 17

3.5.6. Pore size distribution test 17

3.5.7. Grease resistance test 17

4. Results and Discussion 18

4.1. Particle size distribution 18

4.2. Mechanical Properties 19

4.2.1. Mechanical properties of CNF/CNC composite films 19

4.2.2. Mechanical properties of the CNF/PEO composite films: 25

4.2.3. Effects of RH on CNF/PEO composite films 29

4.3. Fourier-transform infrared spectroscopy with attenuated total reflection (FTIR-ATR).. 32

4.4. Atomic Force Microscopy (AFM) 34

4.5. Pore size distribution 37

4.6. Contact angle measurement 38

4.7. Oil and grease resistance 43

5. Conclusions 45

6. Limitations and Future Recommendations 46

References 47

List of tables

Table 3.1	Suspension formulation design for CN-based films	10
Table 3.2	Suspension formulation design for CNF/PEO-based films.	15

List of figures

Figure 1.1.	The SEM images of Kenaf paper made from (a) unbeaten pulp and (b) beaten pulp	4
Figure 1.2.	Oil penetration through plain paper: (a) A droplet of vegetable oil placed on top of a piece of regular paper with another piece of paper placed underneath it, (b) the surface of the underneath paper showing oil contamination	5
Figure 4.1.	Particle size distribution of CNF and CNC suspension	19
Figure 4.2	The thicknesses of the CNF/CNC composite films and commercial paper products.	20
Figure 4.3.	Tensile strength and strain at break of CNF/CNC-based films and commercial products.	22
Figure 4.4.	Tensile energy absorption of CNF/CNC-based films and commercial products.	23
Figure 4.5.	Young's modulus of CNF/CNC-based films and commercial products.	24
Figure 4.6.	Tensile strength and Young's modulus of the CNF/PEO composite films.	25
Figure 4.7.	Tensile energy absorption (TEA) and strain at break of CNF/PEO films.	27
Figure 4.8.	The moisture content of CNF/PEO-based composite films.	28
Figure 4.9.	CNF/PEO composite films at a ratio of 100/0, 95/5, 90/10, 85/15 and 0/100	29

Figure 4.10.	Tensile strength and Young's modulus of the CNF/PEO composite films at 30%, 50%, and 90% RH.	30
Figure 4.11.	Strain at break and Tensile energy absorption of the CNF/PEO composite films at 30%, 50%, and 90% RH.	32
Figure 4.12.	FTIR analysis of CNF/PEO composite films at a ratio of 100/0, 95/5, 90/10, 85/15 and 0/100	34
Figure 4.13.	AFM height images of CNF/CNC composite films at a ratio of 100/0, 85/15, 70/30, 55/45 and 30/70	36
Figure 4.14.	AFM images of CNF/PEO composite films at a ratio of 95/5, 90/10, 85/15 and 0/100	37
Figure 4.15.	Pore size distribution of CNF/PEO composite films at 100/0, 95/5, 90/10, and 85/15ratio	38
Figure 4.16.	Contact angle as a function of time for CNF/PEO composite films using water.	39
Figure 4.17.	Contact angle as a function of time for CNF/PEO composite films using water.	41
Figure 4.18.	Effects of water contact angle on different CNF film thickness as a function of time.	42
Figure 4.19.	Effects of water contact angle on different CNC film thickness as a function of time.	43
Figure 4.20.	Oil and grease resistance test : (a) Before kit test (b) After kit test	44

1. Literature Review

Paper-based materials are the first choice for packaging manufacturing since they have an environmentally friendly tag. There is an increasing demand for the food we regularly consume, like pizza, burgers, and others, which require grease-resistant packaging material for consummation and transportation. In this regard, the paper containing per- and poly-fluoroalkyl substances (PFASs) is the most common and dominates the current market because of its effective resistance to grease, oil, and water. However, the major challenge of using PFASs is being potentially toxic to the environment and health when the paper product closely interacts with food. In search of an alternative, this research work demonstrates a method of preparing grease-resistant food packaging products using cellulose nanomaterials.

1.1. Introduction

The food packaging industry is expanding exponentially and holds the largest share 85% of the overall packaging market (J. Huang, X. Ma, G. Yang 2019). Food processing industries choose packaging materials considering the packaging barrier properties (water, oil, and gas barrier), heat sealability, processability, strength, printability, and cost-effectiveness (Deshwal et al. 2019). In 2015, paper and paperboard production covered 31% of the total packaging market in the world. Paper-based materials have been predominantly used for the food industries where paper contacts directly with food products during packaging. Additionally, industries use paper-based materials for transportation and storage purposes (Khwaldia et al. 2010). These packaging materials help us enjoy our food as they restrict oil or grease from penetrating and reaching our

fingers. Most foods containing oil or grease are commonly handled in paper-based boxes or flexible thin paper possessing grease resistance. For the benefits of food safety and easy processability, grease-resistant paper-based packaging is essential for food handling in our daily life.

Unlike regular paper products, most grease-resistant food packaging paper products are treated with potentially harmful chemicals which are persistent in the environment and pose a significant threat to human health (Azeredo et al. 2017; Mudumbi et al. 2017). Paper containing per- and poly-fluoroalkyl substances (PFASs) is the most common and dominates the current market because it effectively establishes resistance to grease, oil, and water (Tyagi et al. 2019). PFASs are commonly used as a paper coating material to achieve the desired grease resistance (Giatti 1996; Stolpe 1996). However, the major challenge of using PFASs is being potentially toxic to health when the paper product closely interacts with food. Under this circumstance, the fluorochemical can migrate into our food during consumption (Begley et al. 2008; Birnbaum and Grandjean 2015; Blum et al. 2015). PFASs were identified to be responsible for thyroid-related diseases, kidney diseases, developmental toxicity, immunotoxicity, metabolic disruption, and cancer. Furthermore, PFASs are highly persistent when disposed into the environment with the packaging, which causes significant negative impacts on the whole ecosystem (Geyer et al. 2017). In this regard, US manufacturers of these kinds of paper products agreed with US Environmental Protection Agency (EPA) to avoid using long-chain PFASs containing eight carbon chains and above, as it has been identified as the most persistent in nature (Blum et al. 2015; Schaider et al. 2017). On the other hand, shorter-chain PFASs containing six carbon or less, which do not have the same persistency and potential toxicity compared to longer-chain fluorochemicals, have been agreed to be used (Rice 2015). Regardless of the fact that long-chain PFASs are not being used in

the US, they are still being used in other countries around the world (Schaider et al. 2017). However, due to the uncertainty of future regulations, industry and academia are interested in PFASs-free grease-resistant paper products (Anon 2017). To achieve this mission of finding new alternatives, it is essential to understand the fundamentals of grease-resistance properties of paper-based products.

1.2. Mechanisms of grease resistance for paper products

Before understanding the principle of grease resistance paper, it is essential to understand how plain paper works in terms of oil/grease resistance. The plain paper we regularly use is manufactured from pulp fibers that are extracted from raw materials like wood and agricultural residues (Bajpai 2012). There are various stages in the paper manufacturing process. Pulping is a process of generating pulp fibers from raw materials with the help of chemical, mechanical, and thermal treatment or by combining any of these. After pulping, beating, and/or refining treatment are commonly applied to the pulp fibers to increase the surface area of fibers so that the water-holding capacity of fibers and bonding ability between fibers increases without significantly reducing the fiber strength (Deshwal et al. 2019). After beating and refining, the fiber slurry is prepared through the stock preparation process for papermaking (Biermann 1996; Smook 1992). Generally, the plain paper structure is porous with distinct roughness. The porosity of the paper largely depends on the degree of beating/refining (Bajpai 2012). For instance, through beating/refining, the interfiber porosity can be reduced by 30-60% compared to paper made from unrefined pulp fibers (Umair et al. 2020). As shown by the scanning electron microscope (SEM) images in Figure 1.1, paper made from unbeaten pulp showed a clear separation of individual fibers, suggesting no fibrillation on the fiber surface and large pores (Figure 1.1 a).On the other hand, paper made from beaten pulp fibers demonstrated fibrillar bridges, which suggest good

bonding among fibers, leaving smaller pores (Figure 1.1 b). Therefore, the paper made from fibers without fibrillation linkage has a larger pore size, facilitating the oil penetration (Umair et al. 2020).

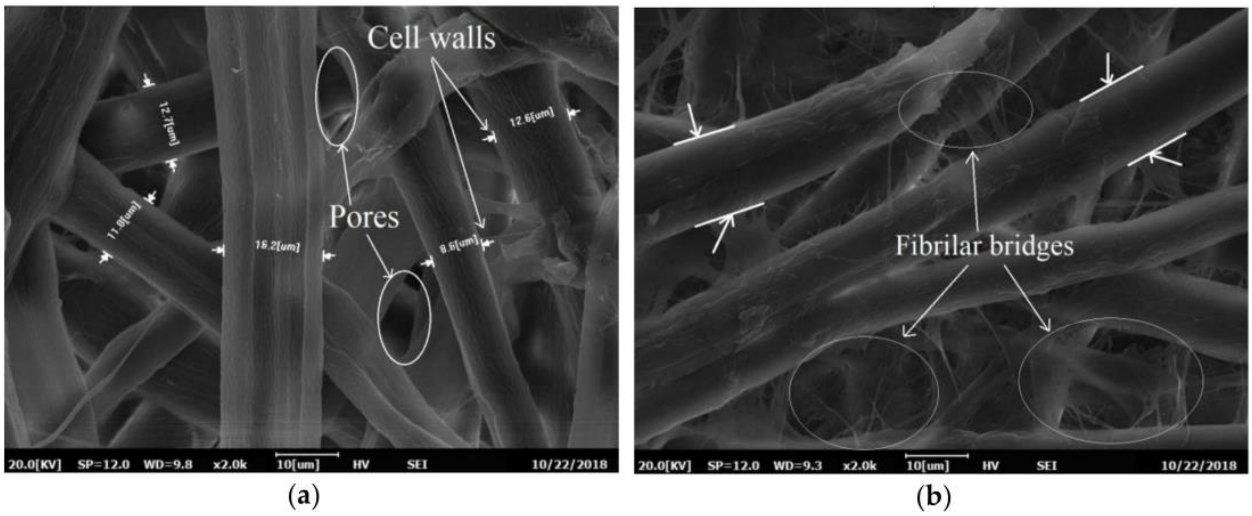

Figure 1.1 The SEM images of Kenaf paper made from (a) unbeaten pulp and (b) beaten pulp (Umair et al. 2020)

An experiment has been performed to observe the phenomenon of oil penetration in plain paper. Two pieces of regular paper were placed on top of each other, and one drop of vegetable oil was placed on the surface of the top paper (Figure 1.2a). Through a light microscope, the immediate penetration of oil into the porous paper structure has been identified in Figure 1.2 (a). After 5 minutes, the bottom paper showed marks of oil contamination (Figure 1.2b).

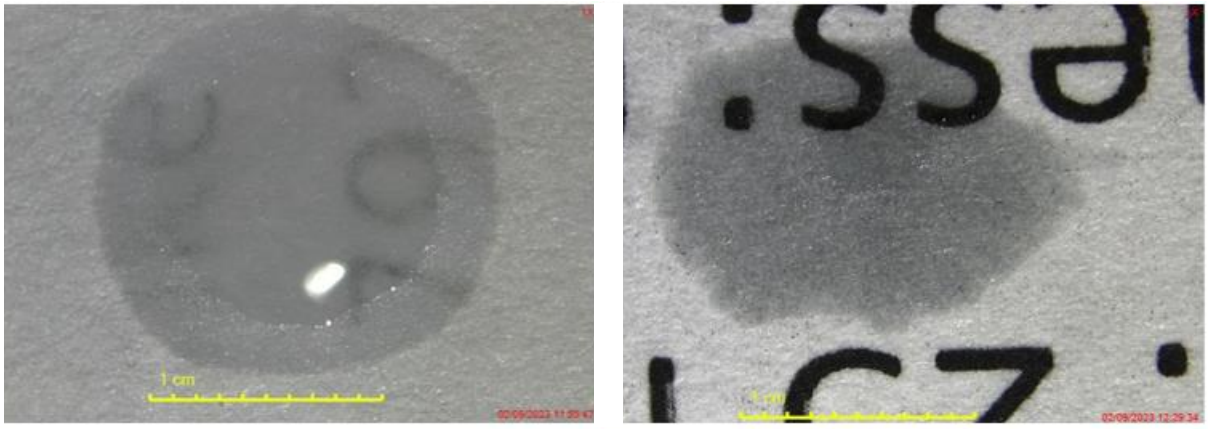

Figure 1.2. Oil penetration through plain paper: (a) A droplet of vegetable oil placed on top of a piece of regular paper with another piece of paper placed underneath it, (b) the surface of the underneath paper showing oil contamination.

From the above discussion, it is understandable that oil penetration occurred due to the porous structure of the plain paper. Hence, to make paper oil/grease resistant, pore sizes in the paper structure have to be reduced by fiber beating/refining. According to Giatti (1996), the main feature of grease resistance comes from a dense surface with few pores on the paper surface. Based on this fact, there is a traditional grease-resistant paper commercially available called glassine or highly refined paper. To manufacture glassine, a high degree of beating is required. In this beating process, many bonding sites on the surfaces of cellulose fibers are created and function as an effective barrier by establishing a hydrogen bonding network during the drying process of papermaking. Hydrogen bond created in glassine paper is more robust in comparison to plastics like polyethylene which use weaker source of forces like van der Waals forces to create the barrier

properties (Castner and Grainger 2001; Griffin 1976; Kjellgren and Engström 2008; Rostami 1998; Song et al. 2015).

Another traditional approach to making grease resistance paper known for around 150 years is parchmentized paper (Mayer 1860). It is also known as vegetable parchment, butter paper, or papyrine (Mayer 1860). The concept was to make the paper dense by pulling a regular paper sheet through a concentrated sulfuric acid, where the paper fibers react with acid and start swelling. During this process, the surface layer of the paper was gelatinized. The follow-up washing and drying steps deposited a dense layer of gelatinized cellulose materials on the paper surface, providing grease resistance (Giatti 1996, Twede and Selke 2004). The parchmentized paper has been widely used for high-end butter and cheese products (Slott-Moller 1972; Lechiffre 1992; Giatti 1996).

The above-mentioned two of the most viable yet economically feasible grease-resistant paper products, namely parchmentized paper and glassine paper, rely on extremely dense paper production. In this paper manufacturing process, a slow water drainage rate and a very long dewatering time are needed, resulting in high energy demand in the drying section. The capacity in the drying section is one of the major limitations for manufacturing grease-resistance paper products in high-speed settings (Anon. 1970). Furthermore, extensive beating is energy and time-consuming, which is another major drawback for producing glassine paper. It has been reported that the beating energy required for making glassine paper is approximately five times higher than for making copy paper (Fellers and Norman 1991). Therefore, using coating material to impart the grease-resistant surface to a piece of regular paper will be an economically viable option compared to manufacturing glassine paper (Kjellgren and Engstrom 2005). Moreover, the energy consumed

to dry a coating layer is one-third of the energy it takes to beat pulp to manufacture uncoated glassine paper (Kjellgren and Engstrom 2005).

In this regard, fluorochemicals have been developed and used as a coating material on the paper substrate to achieve grease resistance properties. The mechanism behind fluorochemicals being grease-resistant, widely known as PFASs or "Forever Chemicals", is low surface energy. PFASs have been used for paper and cardboard since the 1940s and 1950s to provide barrier properties against oil, water, and fat (Ramírez Carnero et al. 2021). Unlike any natural chemicals, PFASs are synthetic chemicals with fluorine atoms covering the carbon molecular backbone. For perfluorinated fluorocarbons, all the carbon atoms are bonded with only fluorine forming C-F bonds with no C-H bonds. For polyfluorinated fluorocarbons, all the carbon atoms form C-H and C-F bonds (Baran 2001; Krafft and Riess 2015). Fluorocarbons have limited ability to bond among themselves or their surrounding molecules. Perfluorinated materials show low surface energy, which prevents them from interacting with their surroundings. The reason behind that is the atomic radius of fluorine (1.47 Å) which is bigger than the hydrogen atom (1.20 Å). Hence, the atomic size of fluorine is very much feasible for shielding the carbon chain from interacting with its surrounding atoms (Krafft and Riess 2015). As a result, PFASs are commonly used by the packaging industry as a surface coating material by leveraging the fluorine atoms' low surface energy and inert nature (Birnbaum and Grandjean 2015). Differing from the other two grease-resistant paper products, which have a closed surface structure with few pores (Stolpe 1986), this PFAS-coated paper has a more open system (Giatti 1996; Stolpe 1996). Hence it can be concluded that for PFAS-coated paper, low surface energy plays a dominant role.

Two mechanisms offering grease resistance to paper products can be summarized from the previous literature review. Firstly, grease resistance can be achieved either by blocking/minimizing

the pores through a high degree of pulp beating or by making the paper surface dense with acid treatment. Secondly, grease-resistant paper surfaces can also be achieved by applying low surface energy coating material. Our research focuses on using cellulose material on a nano-scale to establish a thin and dense layer on a regular paper surface to impart the desired grease resistance. In the next section, we will review the potential of using cellulose nanomaterials (CNs) to achieve grease resistance.

1.3. New strategies to develop grease-resistant paper products

Although PFASs coated paper is potentially toxic to our health and the environment, the coating technique used for PFASs is an economically viable way to make convenient grease-resistant paper products. Hence, in this study, we will be developing CN-based coating for a paper to develop grease resistance. CN is a non-toxic, sustainable, and renewable nano-scaled cellulosic material (Phuong et al. 2022). Cellulose is the most abundant polysaccharide in nature, encapsulated by lignin and hemicellulose. It is a linear chained structure with a repeated unit of β-(1→4)-D-glucopyranose (Hubbe et al. 2017). The cornucopia of cellulosic biomass around us and their outstanding mechanical properties made them desirable for nanocomposites incorporated with other polymers (Hubbe et al. 2017). CN is produced from natural cellulose sources (wood, grass, cotton, tunicate, etc.) by chemical treatment, mechanical treatment, or a combination of chemi-mechanical treatment or bacterial production (Omran et al. 2021). Three major types of CNs have been studied intensively in the literature, including cellulose nanofibrils (CNFs), cellulose nanocrystals (CNCs), and bacterial cellulose (BC) (Ferrer et al. 2017). CNFs and CNCs are mainly produced from wood cell walls, whereas BC is produced from bacteria (Nechyporchuk et al. 2016). The major limitation of using BC is that it is resistant to biodegradation in the absence of cellulolytic enzymes (Roman et al. 2019). Hence, this study will only focus on CNFs and CNCs.

In terms of appearance, CNFs have a spaghetti-like shape, while CNCs have a rice-like form. CNCs can be packed more densely than CNFs (Wang et al. 2020). CNFs have a diameter of 10 to 100 nm and a length of several microns, while CNCs are rigid nanomaterials having a diameter of 5 to 20 nm and a length of 100 to 200 nm (Vergara-Figueroa et al. 2022). In terms of mechanical properties, CNs possess superior properties; for instance, CNFs have a tensile strength of 7.5-7.7 GPa, Young's modulus of 110-220 GPa, and CNCs have a tensile strength of approximately 10 GPa and Young's modulus of approximately 110-130 GPa. CNs also have biodegradability, tunable surface chemistry, excellent chemical resistance ability, and renewability (Chen and Hu 2018; Chen et al. 2018; Moon et al. 2011; Shojaeiarani et al. 2021; Thomas et al. 2018).

Many research articles handling CNs for food packaging applications have been focused on their barrier properties (Choi and Simonsen 2006). Four types of barrier performance were commonly studied for CN films in packaging: oxygen barrier, oil/grease barrier, water barrier in vapor form, and liquid form (Hubbe et al. 2017). However, in this study, we will be focusing on the oil/grease barrier performance of CN-based films due to the importance of such a topic in packaging applications. Several studies were conducted addressing oil/grease barrier properties of CN-based films (Aulin et al. 2010; Kisonen et al. 2015; Kumar et al. 2014; Österberg et al. 2013; Sirviö et al. 2014).

CNCs have recently been used in a grease resistance formulation with sodium montmorillonite (MMT) and soy protein (Tyagi et al. 2018). It was reported by Tyagi et al. (2018) that paper coated with only CNCs failed kit rating 1 while the mixture of CNCs incorporated with MMT, soy protein, and alkyl ketene dimer-coated paper passed kit rating 6. It was reported by Hubbe et al. (2017) that, to achieve good oil/ grease barrier properties, CNFs played roles in the coating process as a stabilizer, pore filler, thickener, and binder and concluded that placing CNFs

onto the porous surface of paper basically seals/decrease most of the pores of the paper. Food packaging materials are expected to show considerable resistance to oil and grease. Interestingly, it was demonstrated that CNF films prepared for oxygen barrier performance tend to provide excellent oil/grease resistance (Kisonen et al. 2015). Another review of published work (Hubbe et al. 2017) suggests that the high cohesive energy density provided by the large network of hydrogen bonding within a pure CN film might be required to achieve effective resistance against oxygen and oils.

2. Problem statement and significance of the study

Despite being a promising alternative to replace potentially toxic and non-biodegradable compounds, CN has certain limitations that hold back its uses in many cases. One of the primary limiting factors is having cracks/pinholes of CN films/coating materials. It was reported that even a highly dense cellulosic film with extensive internal hydrogen bonding networks could be expected to give poor barrier performance if it has pinholes or cracks. For instance, it was reported that four layers of starch-PVOH were necessary to cover glassine paper to avoid any effects of pinholes or cracks (Javed et al. 2017). Theoretically, a higher crystallinity is desirable to achieve good barrier properties for the CN films (Kjellgren et al. 2006). However, high crystallinity results in the brittleness (easy to crack) of the film. Due to the higher crystallinity in CNCs compared to CNFs, films prepared with only CNCs are brittle and difficult to handle(Fernández-Santos et al. 2022). To address this issue, sorbitol, a plasticizer, was used to increase the flexibility of CNC films (Bardet et al. 2015). However, the tensile strength of the CNC films with plasticizer decreased significantly. Another approach reported by Tyagi et al. (2018) is to incorporate MMT into CNC-based film formulation. The MMT incorporation into CNC suspension successfully increased the coated paper's stiffness by 20% compared to uncoated paper. Due to the high

crystallinity of MMT, soy protein was added to improve CNC-MMT coating behavior with a hydrophobic agent alkyl ketene dimer (AKD) in cationic emulsion form. This coating recipe improved grease resistance ability by reaching a kit rating of 6 while only CNC-coated paper failed the lowest kit rating of 1. However, a higher kit rating couldn't be achieved with this mentioned coating recipe due to the brittleness of the coating layer. Furthermore, a complex formulation with multiple chemical components, including CNC, MMT, protein, and AKD, is necessary for the coating formulation which complicates the system. Therefore, future research focused on more practicable film formulation to resist oil and grease at a higher kit rating needs to be developed.

Another primary concern with CNFs for packaging applications is their hydrophilicity due to their amorphous structure and the presence of surface hydroxyl groups. It has been reported that at higher relative humidities, the barrier properties of CNF films become suppressed (Miettinen et al. 2014). On the other hand, CNC-containing composites show less sensitivity to humidity when compared to CNFs (Nair et al. 2014). Herein, considering the different attributes of CNCs and CNFs, we hypothesize that desired properties in grease resistance can be achieved by combining them. Hence, our study focused on preparing CN-based films by mixing CNFs and CNCs at different ratios to optimize the film properties.

To further address the problems of pinholes and high sensitivity towards humidity of the CN-based films, we incorporated polyethylene oxide (PEO) in the CN film formulation development. PEO is a linear structured, semicrystalline, and water-soluble polymer (Harris 2013; Zhou et al. 2011), and is used widely in the field of tissue engineering, solar energy utilization, waste heat recovery, electric energy storage, and drug-controlled release (Chen et al. 2015; Fallahi et al. 2017; Li et al. 2009; Liang et al. 1995; Peng et al. 2016). It was reported by Shi et al. (2019) that the standalone film of PEO incorporated with CNFs formed new hydrogen bonds and resulted

in highly dimensionally stable films. Therefore, in this study, PEO was added with CNs to the formulation development process to understand the contribution of PEO to mechanical properties, physical properties, pore size distribution, and grease resistance of the prepared films.

3. Materials and methods

3.1 Raw material

The CNF suspension (3 wt.%) was purchased from the Process Development Center (PDC) at the University of Maine (Orono, ME, USA). The CNC suspension (6 wt.%) was purchased from CelluForce Inc. (Montreal, Quebec, Canada). The suspensions of CNF and CNC were diluted using deionized (DI) water to prepare the 1 wt% suspensions. During the dilution process, a homogenizer (IKA T25 digital Ultra-Turrax, IKA works Inc, Wilmington, NC, USA) was used to disperse the CNF or CNC in the suspension at 3000 revolutions per minute (rpm) for 3 min, followed by stirring overnight using a magnetic stirrer for 12 hours at room temperature condition (22ºC, 50% RH). Parafilm was used to cover the beaker top to prevent water evaporation during the stirring process. The PEO powder, at a weight average molecular weight between 250,000 to 400,000, was supplied by Thermo Scientific Chemicals (MA, USA). A 4 wt.% PEO solution was prepared by dissolving 4 g PEO in 96 g of DI water by stirring the mixture for two days at room temperature. Commercial paper products, including parchment paper sheets (Reynolds Kitchens, USA), copy paper (Worklife Brands LLC, Massachusetts, USA), pan liner from unbleached paper (LO10U, DIXIE, USA), and FDA-approved butcher paper (5PGK9, Grainger, Lake Forest, IL, USA), were purchased for this research.

3.2. Particle size distribution

The particle size measurements of CNF and CNC were carried out using dynamic light scattering (DLS) technology with a Litesizer^{TM} 500 (Anton Paar, Ashland, VA, US). Suspensions of CNF and CNC at 0.01 wt.% were prepared for the particle size analysis. The instrument uses a 40 mW semiconductor laser operating system at a wavelength of 658 nm. The light scattering was detected at 90º by backscattering technology. Results were presented as an average value of five experiments for each sample.

3.3. Standalone CNF/CNC composite films

Standalone films were prepared by mixing CNFs and CNCs at 1 wt.% concentration according to the formulation design shown in Table 1. The aqueous CNF and CNC suspensions were mixed using a high-speed homogenizer at 3000 rpm for 5 minutes. The mixture was then stirred for 12 hours at 750 rpm at room temperature to remove the air bubbles using a magnetic stirrer. Afterward, the suspensions were cast on a 120 mm x 120 mm polystyrene petri dish and allowed to dry at room temperature for seven days to reach equilibrium with room conditions. For each film preparation, 60 grams of suspension was used consistently. After drying, the films were cut into strips with dimensions of 25.4 mm width and 101.6 mm length with a lab film cutter according to the ASTM standards D828 for mechanical property characterization. All the commercial paper products were cut into strips with the same dimensions for characterization.

Table 3.1. Suspension formulation design for CN-based films

CNF (1 wt% suspension)	CNC (1 wt% suspension)
100	0
85	15
70	30
55	45
30	70

3.4. Standalone CNF/PEO composite films

The CNF/PEO composite films were prepared by mixing CNF suspension (1 wt.%) and PEO solution (4 wt.%) according to the formulation design shown in Table 2. The CNF suspension and PEO solution were mixed using the same procedure as preparing the CNF/CNC composite films. The CNF/PEO suspension casting was similar to the CNF/CNC composite films mentioned earlier. The films took seven days to dry in room conditions. Next, films were oven dried at 105 °C for 6 hours, then conditioned for one hour at room temperature before mechanical characterization. PEO used in this study has a melting temperature of 65 °C (Fischer 2020). At first, the films were dried in the oven at 80 °C, 105 °C, and 120 °C for 6 hours. As PEO has a melting temperature of 65 °C therefore, it is important to ensure that PEO is melting properly inside the films to flow around the pores of CNFs. Films dried at 80 °C swelled when contacted with water, while films dried at 105 °C and 120 °C showed stability. Therefore, 105 °C has been

chosen as the optimum oven drying temperature to dry the films. The CNF/PEO composite films were prepared with the CNF suspension to the PEO solution of 95/5, 90/10, and 85/15 ratios. After drying, the theoretical PEO contents in the solid films were 17%, 30%, and 41%, corresponding to the CNF suspension to the PEO solution ratios of 95/5, 90/10, and 85/15.

Table 3.2. Suspension formulation design for CNF/PEO-based films.

CNF (1 wt% suspension)	PEO (4 wt% solutions)	PEO solid content (%)
100	0	0
95	5	17
90	10	30
85	15	41

3.5. Characterization of films:

3.5.1. Mechanical properties

The mechanical properties, including tensile strength (TS), strain at break, tensile energy absorption (TEA), and Young's modulus, of all the prepared films and commercial paper products were tested using a Mark-10 motorized force test stand ESM750S (Copiague, NY, USA) accompanied with a 500 N load cell at 22°C and 50% RH. The initial grip distance was 25.4 mm, and the grip separation rate used was 7 mm/min. Ten replicates of each sample were measured to report the film properties. The thicknesses of each specimen and the commercial product were measured using a digital micrometer screw gauge (model 293-831-30, Mitutoyo, Japan). The mechanical properties of all the tested samples, including TS, strain at break, TEA, and Young's modulus, are reported according to the ASTM standard D828. Moisture content was measured

with seven replicates for each sample by drying them at 105 °C until constant weight. A statistical analysis of the mechanical properties and moisture content of all the samples was also carried out.

3.5.2. Contact angle measurement

The water contact angle of all the films was measured by using a contact angle goniometer (Ossila Contact Angle Goniometer, UK) at room temperature with 50% RH. The contact angle determines the wetting degree between a liquid and a solid. High contact angle (> 90 °) represents hydrophobicity and vice versa. During contact angle measurement, the appropriate size of the film was bonded to the top of a glass slide using double-sided tape. For each test sample, contact angle measurements were performed ten times at different locations. The contact angle changes of water droplets on the film surface were captured with time. The contact angle data were extracted at 0.5, 1, 2, 3, 4, and 5 minutes, counting from when the water droplet contacted the film surface. The water contact angle measurement procedure followed the literature (Wang et al. 2020).

A separate set of experiments were performed to understand the effect of film thicknesses on surface properties using contact angle analysis. Films were prepared by casting 20g, 40g, 60g, and 80g of the 1 wt.% CNF and CNC suspensions in petri dishes. After drying at room temperature condition (22°C and 50% RH) the thickness of the films for 20g, 40g, 60g, and 80g were measured. Films with different thicknesses were used to evaluate the changes in the water contact angle. The contact angles were measured from 30 sec to 5 min after the contact between the probing liquid (water) and the film surface.

3.5.4. Atomic Force Microscopy (AFM)

A Bruker Dimension Icon AFM (Bruker Nano Inc., Santa Barbara, CA, USA) was employed in this work. The ScanAsyst mode was employed to investigate the morphology of the

film surfaces. ScanAsyst-Air probes were used. The nominal probe spring constant and radius were 0.4 N/m and 2 nm, respectively. The probes were calibrated by the thermal tune method before use. Five random areas (2 μm × 2 μm) were imaged on each surface. The data were processed with the software NanoScope Analysis 2.0 (Bruker) and height images were generated.

3.5.6. Fourier-transform infrared spectroscopy with attenuated total reflection (FTIR-ATR)

The chemical bonding structures of the film samples of CNF/PEO at 100/0, 95/5, 90/10, 85/15, and 0/100 were characterized by FTIR-ATR using a Perkin Elmer Spectrum 400 FTIR spectrometer equipped with deuterated triglycine sulfate (DTGS) detector and a built-in Perkin Elmer ATR module (diamond-selenium crystal). Before the measurements, a background spectrum was recorded for each different sample. Next, all spectra were collected from 500 to 4000 cm^{-1} with a 4 cm^{-1} wavenumber resolution after 64 continuous scans.

3.5.6. Pore size distribution test

The pore size distribution of the films at 100/0, 95/5, 90/10, 85/15, and 0/100 of CNF/PEO were measured using a capillary flow porometer (CFP- 1200-AEXM, Porous Materials Inc, city, state, USA). The procedures using the capillary flow porometer followed the method in the literature (Jang and Kang 2020).

3.5.7. Grease resistance test

A grease resistance test (the Kit test) was performed by following the TAPPI test Method T559 cm-12 to test the degree of repellency of the films against oil and greasy substances. This test uses a series of 12 solutions with different ratios of castor oil to the mixture of toluene and n-heptane. The aggressiveness of the test solutions increases with the increasing content of n-heptane and decreasing content of castor oil. A drop of a chosen kit solution was placed on a film at a

height of about 13 mm above the film using an eye-dropper. A piece of kraft paperboard in brown color was placed under the film to observe the penetration of the solution. After 15 s, the droplet was removed from the film, and any darkening of the underlying paperboard resulted in the "failure" of the test. The test continued until the highest kit number was obtained and reported as the Kit number of the film.

4. Results and Discussion

4.1. Particle size distribution

The particle size distributions, as measured by DLS, of CNF and CNC are shown in Figure 4.1. The CNFs are mechanically extracted fibrous materials with a large aspect ratio, while the CNCs are chemically extracted needle-like materials. The CNC shows a single peak at around 100 nm (from 47.6 to 260 nm), while the CNF shows two peaks at around 200 nm (from 126 to 300 nm) and 1300 nm (from 690 to 2000 nm). The minimum particle sizes of the CNC and CNF particles in the suspensions were around 47 nm and 126 nm.

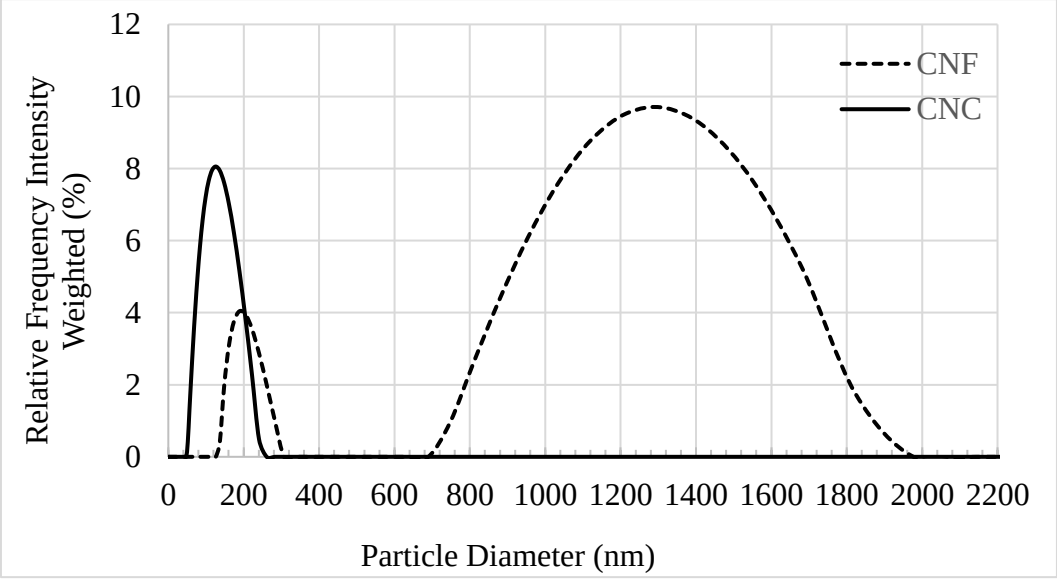

Figure 4.1. Particle size distribution of CNF and CNC suspension

4.2. Mechanical Properties

4.2.1. Mechanical properties of CNF/CNC composite films

Several commercial paper products, namely parchment paper, butcher paper, pan liner, and copy paper, were tested as control samples to compare with the CNF/CNC composite films. The thicknesses were measured for all the CNF/CNC composite films and commercial papers (Figure 4.2). Parchment paper has a thickness of 0.05 (±0.01) mm, similar to the pure CNF films with a thickness of 0.052 (±0.02) mm. In addition, parchment paper is a traditional grease-resistant paper that doesn't contain fluorochemicals. Therefore, in this section, the mechanical properties of parchment paper were treated as the benchmarks to be compared with the CNF/CNC composite films and were further compared with other commercial paper products.

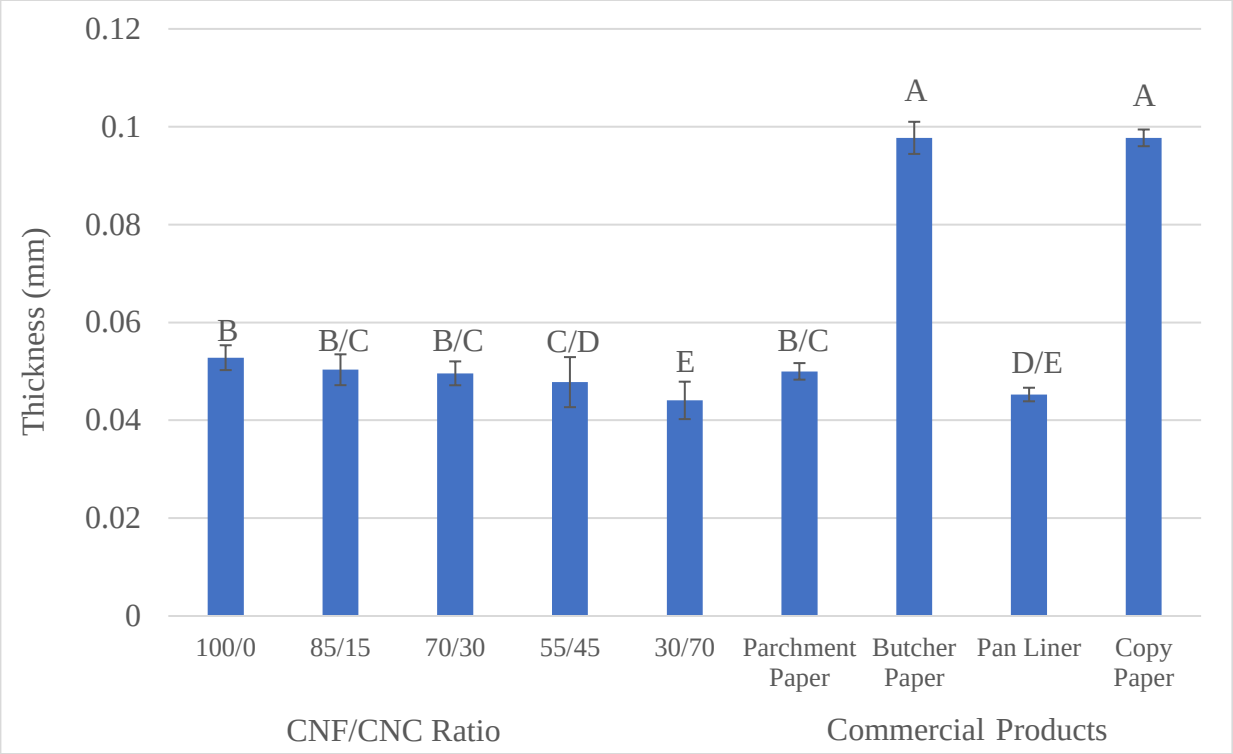

Figure 4.2. The thicknesses of the CNF/CNC composite films and commercial paper products.

The letters A, B, C, D, and E represent the significant levels in statistical analysis. The values with different letters are significantly different. Throughout the whole thesis paper, the letters will carry the same meaning as mentioned.

TS values and the strain at break values for all the CNF/CNC composite films and commercial paper products are shown in Figure 4.3. The TS values of the CNF/CNC composite films with up to 30 wt.% CNC are not significantly different from the 100 wt.% CNF films. As the weight ratio of CNC in the composite film increased to 45 and 70%, the TS significantly decreased. The TS value of the 100 wt.% CNF film is 103 ± 11.0 MPa which is nearly 39.8% higher than that of the film containing the highest CNC loading (70 wt.%), which is 73.9 ± 4.3 MPa. The TS value of 100% CNF film is 41.4% higher than parchment paper (72.8 ± 5.5 MPa). The composite film

with 45 wt.% of CNC showed a higher TS value than the parchment paper, while the 70 wt.% of CNC-loaded film showed a similar TS value to the parchment paper. The TS value of parchment paper is much higher than butcher paper, pan liner, and copy paper, which have TS values of 50.7 ± 3.2 MPa, 38.6 ± 2.8 MPa, and 19.7 ± 0.7 MPa, respectively. Similarly, the 100 wt.% CNF film exhibited the greatest strain at break (12.7 % ± 0.02), which is more than twice the highest CNC-loaded film (5.6 % ± 0.03). According to Wang. L (2020), the lower the crystallinity of the cellulose-based film material, the greater the strain at break. As mentioned earlier, CNC is a higher crystalline polymer compared to CNF. Therefore, films prepared with a higher CNC loading level result in lower TS and strain at break. In addition, the strain at break value of 100% CNF films is four times higher than the parchment paper (2.5%). The CNF/CNC composite films at the CNF/CNC ratios of 85/15, 70/30, 55/45, and 30/70 have strain at break values of 11.4 ± 0.01, 9.7 ± 0.01, 8.5 ± 0.07, and 5.6% ± 0.07, respectively. The strains at the break for these films are all greater than that of parchment paper. Furthermore, the strain at break value of the parchment paper is similar to the butcher paper (3.1% ± 0.02) but lower than those of pan liner (5.8% ± 0.07) and copy paper (5.8% ± 0.01). A similar trend was observed for the TEA values shown in Figure 4.3. The films prepared with 100 wt.% of CNF have a TEA value of 9060 J/m^3 (± 2076.8), which is more than double that of the highest CNC-loaded film (3260 ± 571.8 J/m^3) and around nine times higher than the parchment paper (1143.3 ± 205 J/m^3). The TEA value of the parchment paper is not significantly different from the pan liner, butcher paper, and copy paper, which have TEA values of 1143.3 ± 834, 993.1 ± 152.7, and 863.1 ± 98.7 N/mm^3, respectively.

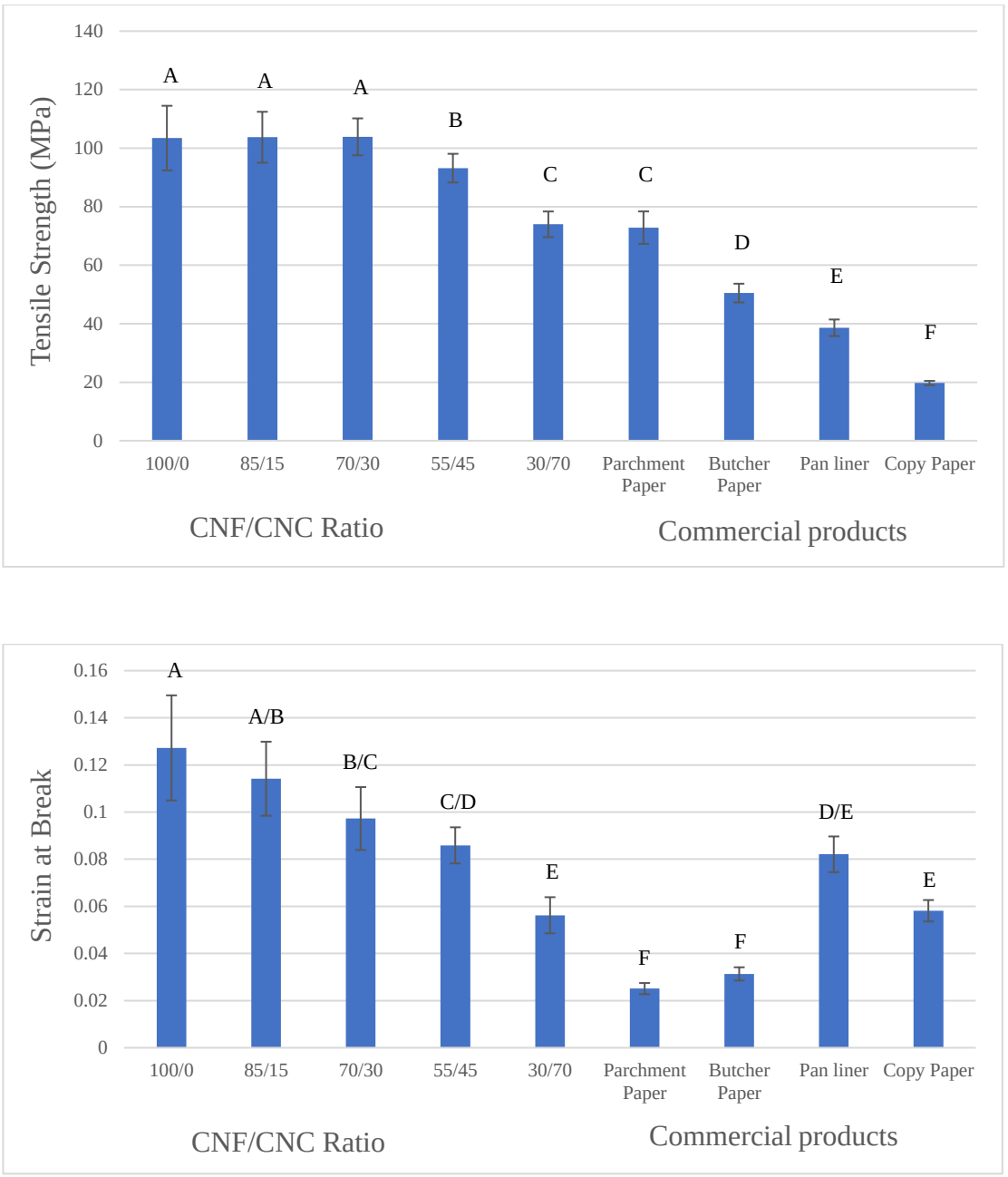

Figure 4.3. Tensile strength and strain at break of CNF/CNC-based films and commercial products.

The addition of CNC increased the film's stiffness, which can be demonstrated by the changes in Young's modulus of the films shown in Figure 4.5. The film with 70 wt.% of CNC has Young's modulus of 6.13 ± 0.39 GPa, much higher than that of the 100 wt.% CNF film (3.24 ± 0.28 GPa). This is probably caused by the higher loading level of CNC, which has a higher degree of crystallinity and densification of the film (Leppänen et al. 2022). Densification of the composite film with 70 wt.% CNC can also be demonstrated from the slightly reduced thickness of such films shown in Figure 4.2. The pure CNF film has a thickness of 0.053 mm, while the composite film with 70 wt.% of CNC has a thickness of 0.044 (± 0.03) mm. Young's modulus value of parchment paper is 5.47 GPa which is not significantly different from the 70 wt.% CNC-loaded film but much higher than the rest of the CNF/CNC composite films. In addition, Young's modulus value of parchment paper is higher than butcher paper, pan liner, and copy paper, which have values of 2.6 ± 0.22 GPa, 1.95 ± 0.31 GPa, and 1.62 ± 0.11 GPa, respectively.

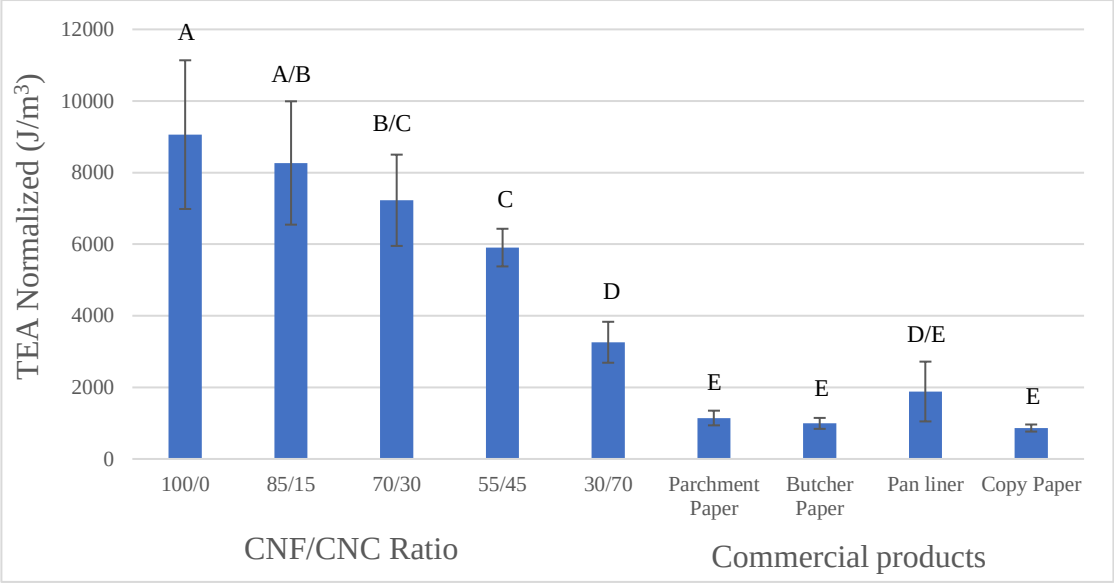

Figure 4.4. Tensile energy absorption of CNF/CNC-based films and commercial products.

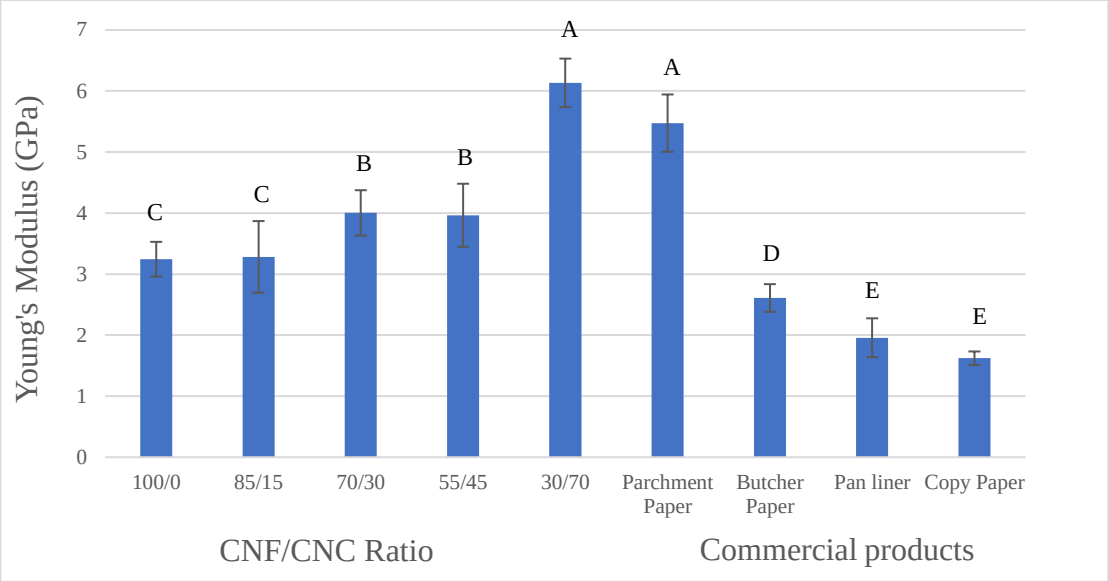

Figure 4.5. Young's modulus of CNF/CNC-based films and commercial products.

Overall, the 100% CNF film showed higher TS and TEA values and lower Young's Modulus value compared to the highest CNC-loaded film and all the other commercial products, including parchment paper. Surprisingly all the CNF/CNC composite films showed higher flexibility (higher strain at break values) than parchment paper. Flexibility is one of the important criteria for food packaging application since the packaging material needs to be folded in a certain pattern. All the CNF/CNC composite films with CNC content up to 45 wt.% showed lower Young's modulus value than that of parchment paper. The Young's modulus value of the film with the CNF/CNC ratio of 30/70 was similar to the parchment paper. The 100% CNF film formulation has been chosen for further study to prepare a coating formulation using PEO since films prepared with only CNF offered greater flexibility in comparison to other films and commercial paper products (Mo et al. 2021).

4.2.2. Mechanical properties of the CNF/PEO composite films:

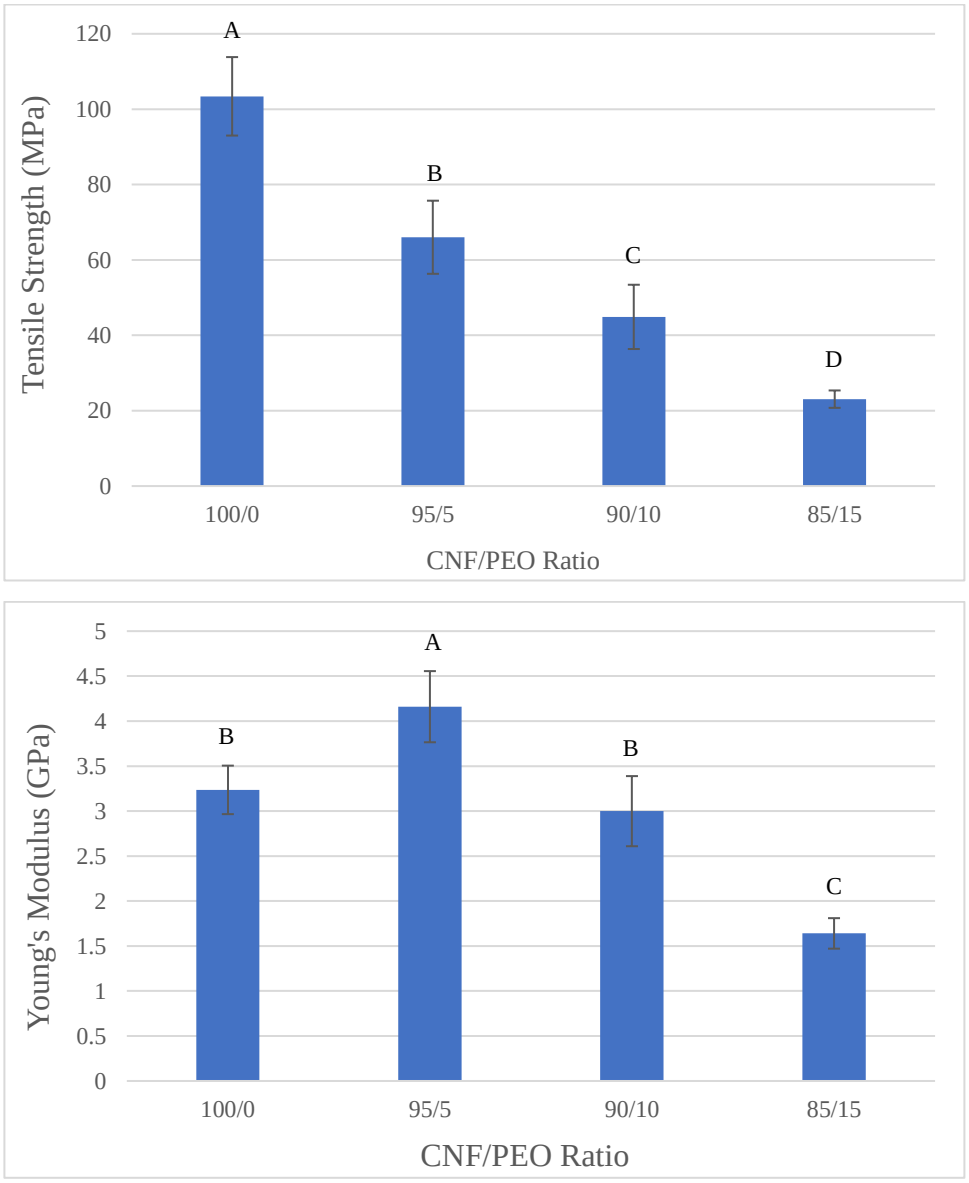

Figure 4.6. Tensile strength and Young's modulus of the CNF/PEO composite films.

The TS of the CNF/PEO composite films decreased with increasing PEO content. For the 100% CNF film, the TS value is 103 ± 11 MPa. The TS of the composite films with PEO decreased to 64.16 ± 0.07 MPa (1.6 fold), 37.78 ± 0.03 MPa (2.7 fold), and 23.06 ± 0.07 MPa (4.5 fold) with

PEO solid content addition of 17%, 30%, and 41%, respectively. The Young's modulus of the CNF/PEO composite film changed significantly with the PEO content of 17% (Figure. 4.6). As PEO content gets higher in the CNF/PEO composite films, the Young's modulus value decreased significantly. For example, the Young's modulus decreased to 2.67 ± 0.27 GPa and 1.64 ± 0.16 GPa after adding 30 and 41 wt.% PEO, respectively.

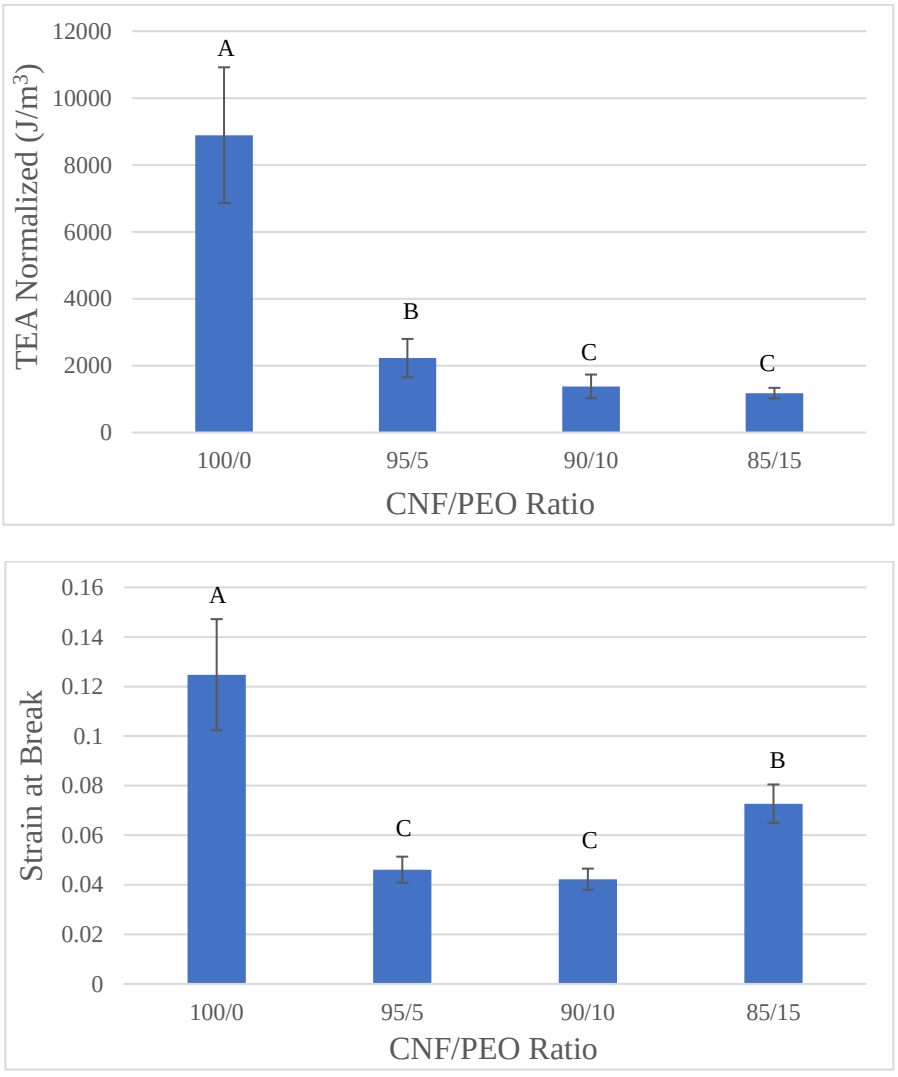

Figure 4.7. Tensile energy absorption (TEA) and strain at break of CNF/PEO films.

On the other hand, the TEA of the CNF/PEO composite films decreased significantly after adding PEO into the film formulation (Figure. 4.7). For 100% CNF film, the TEA decreased from 9059 J/m^3 ± 2076.7 to 2225 ± 284.1 J/m^3 (3 fold), 1377 ± 157.3 J/m^3 (5.5 fold), and 1178 ± 157.3 J/m^3 (6.7 fold) for the films containing 17, 30, and 41 wt.% of PEO, respectively. The pure PEO films were brittle and broken into pieces while peeled off from the petri dish, as shown in Figure 4.9. According to Li & Matsuba (2019), the PEO crystallization process correlates with temperature and the PEO crystallization process accelerates as the annealing temperature increases. All the CNF/PEO composite films were dried in an oven at the temperature of 105°C for 6 hours. This process possibly increased the crystallinity of PEO, resulting an increase in brittleness. Therefore, it is possible that with increasing PEO loading levels, the brittleness of the CNF/PEO composite films increased, which lowered the tensile strength and TEA values. Similarly, the strain at the break value of the CNF/PEO films decreased two-fold from 13% to 5% after adding 17 wt.% PEO in the pure CNF film formulation. After adding 30 wt.% PEO the strain at break decreased to 4% ± 0.01, which is not significantly different from the 17 wt.% PEO addition in the CNF film formulation. However, the addition of 41 wt.% PEO surprisingly increased strain at break property to 7% ± 0.02. This could be due to the increment of moisture content in CNF/PEO films (Figure 4.8). PEO is a nonionic hydrophilic material (Vanza et al.). As the PEO content increased in the film (Figure 4.8), the moisture content of such films also increased. CNF/PEO composite film at the PEO content of 17 wt.% showed 9.3 ± 2.7 wt.% moisture content which is significantly different than 100% CNF film showing a moisture content of 5.5 ± 0.3 wt.%. Moreover, further addition of PEO increased moisture content. For example, the CNF/PEO composite films with 30 and 41 wt.% PEO showed moisture contents of 10 ± 1.0 and 14.7 ± 1.9 wt.%, significantly greater than the other two films.

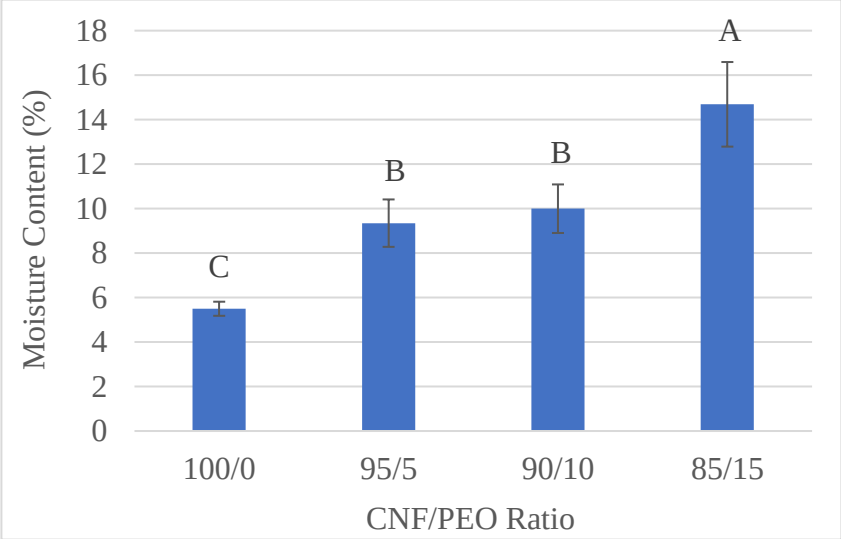

Figure 4.8. The moisture content of CNF/PEO-based composite films.

The increased moisture contents in the CNF/PEO composite films led to lower TS properties and greater strain at break values. The reason behind this observation is that the absorption of moisture weakens the bonding strength between CNFs due to the reduction of hydrogen bonds, resulting in easier interfacial debonding and sliding between CNFs (Benítez et al. 2013; Wang et al. 2018).

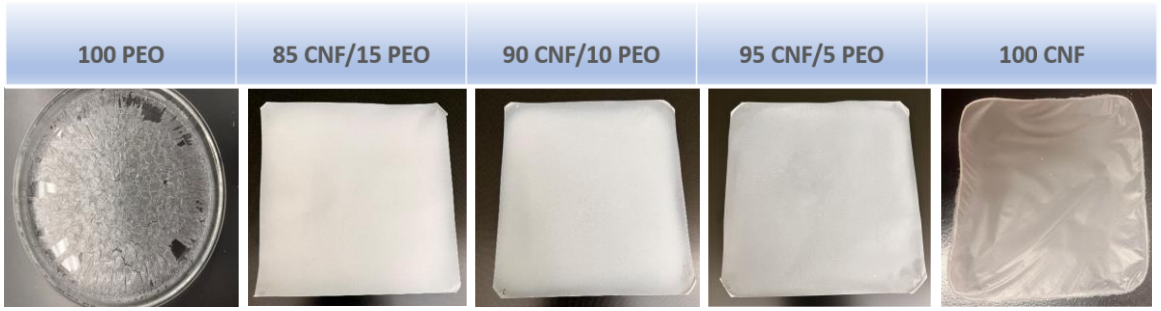

Figure 4.9. CNF/PEO composite films at a ratio of 100/0, 95/5, 90/10, 85/15 and 0/100

4.2.3. Effects of RH on CNF/PEO composite films

The CNF/PEO composite films conditioned at 30, 50, and 90% RH were tested to understand the effect of RH on film mechanical properties (Figure 4.10. The mechanical properties of CNF films are moisture-sensitive (Wang S et al. 2018; Sehaqui H et al. 2014; Benitez A et al. 2013; Osterberg M et al. 2013). As the RH increases, the TS value and Young's modulus decrease, and the strain at break increases. The TS values at 30% and 50% RH are not significantly different for all the CNF/PEO composite films. However, at 90% RH, the TS value drastically decreased. For example, at 90% RH, the TS value for 100% CNF film decreased from 103 ± 11 MPa to 80 ± 16.3 MPa, which is 27% lower than the film conditioned at 50% RH. Similarly, at 30% RH, the CNF/PEO composite films showed decreased TS values of 64 ± 7.6 MPa, 37 ± 12.3 MPa, and 24 ± 5.5 MPa at 95/5, 90/10 and 85/15 ratios, respectively. Young's modulus value of 100% CNF film at 50% RH is not significantly different from that at 90% RH. However, at 90% RH, Young's modulus values decreased for all the CNF/PEO composite films. Since CNF and PEO are both hydrophilic materials, it can be concluded that after adding PEO into the CNF matrix, films became more moisture sensitive than pure CNF films, further weakening film properties at high RH levels.

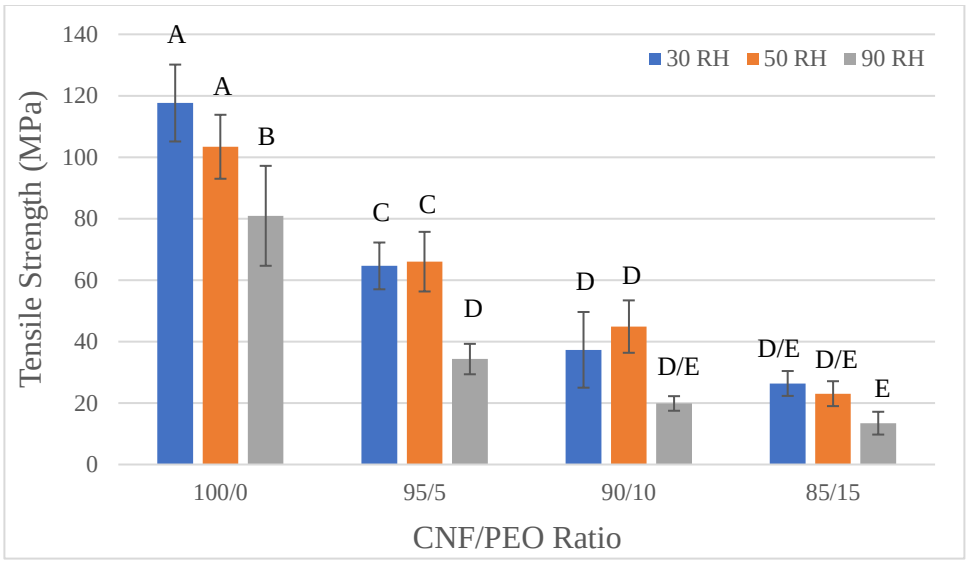

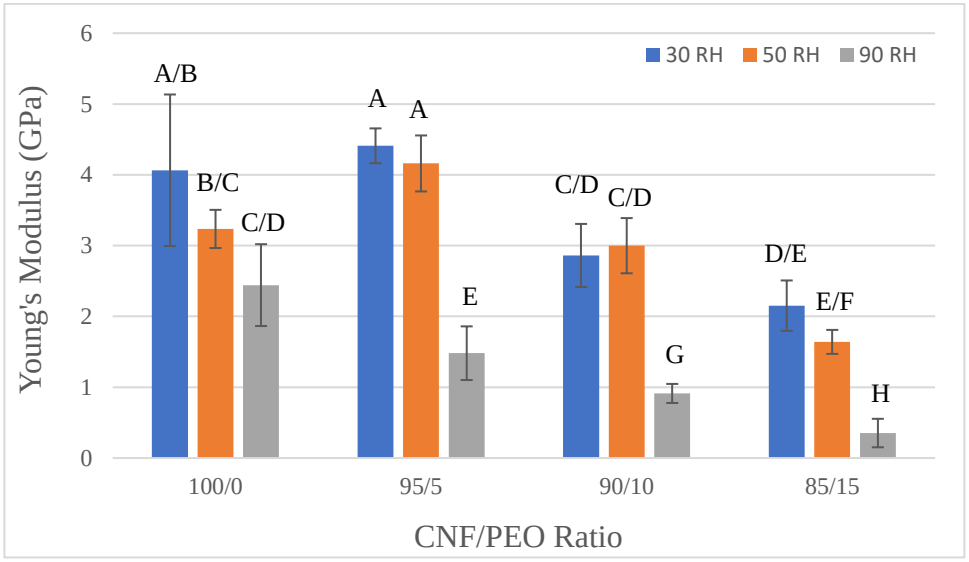

Figure 4.10. Tensile strength and Young's modulus of the CNF/PEO composite films at 30%, 50%, and 90% RH.

The TEA and strain at break values of all CNF/PEO composite films are shown in Figure 4.11. The TEA value of 100% CNF films decreased at 90% RH, and the values are significantly different from that at 50% RH. However, the TEA values for all CNF/PEO films are not

significantly different at the three RH levels. In contrast, the strain at break value increased at 50% RH compared to 30% RH for the film with 41 wt.% PEO, and the values are not significantly different for all the other films at 30 and 50 % RH levels. However, at 90% RH, the strain at break values are significantly different from 50% RH for all the films. For example, at 50% RH, the CNF/PEO film with 17 wt.% PEO has the strain at break value of 3% ± 0.03, which increased to 9% ± 0.08 (twice) at 90% RH. Similarly, the strain at break values increased from 3.6 % ± 0.04 and 7.2 % ± 0.07 to 6.7% ± 0.06 and 10.5% ± 0.02 for films with 30 wt.% and 41 wt.% of PEO.

The main reason behind such an increment in strain properties and decrease in TS values is associated with the moisture sorption properties of the hydrophilic films, resulting in the swelling of the CNF and PEO. The swelling of CNF and PEO molecules led to the larger deformation under external load, simultaneously lowering interfibrillar stress transfer and TS (Benitez et al. 2013). In addition, secondary interactions dominate the work of adhesion between CNFs in the dry state, and this will be reduced if a sufficient amount of water hinders the interfibrillar bonding, further decreasing the TS (Henriksson et al. 2008; Meng and Wang 2019). In addition, the flexibility of fibers and molecules caused by water swelling promotes interfibrillar shearing and sliding, accelerating the decrease of the TS (Meng et al. 2019; Henriksson et al. 2008).

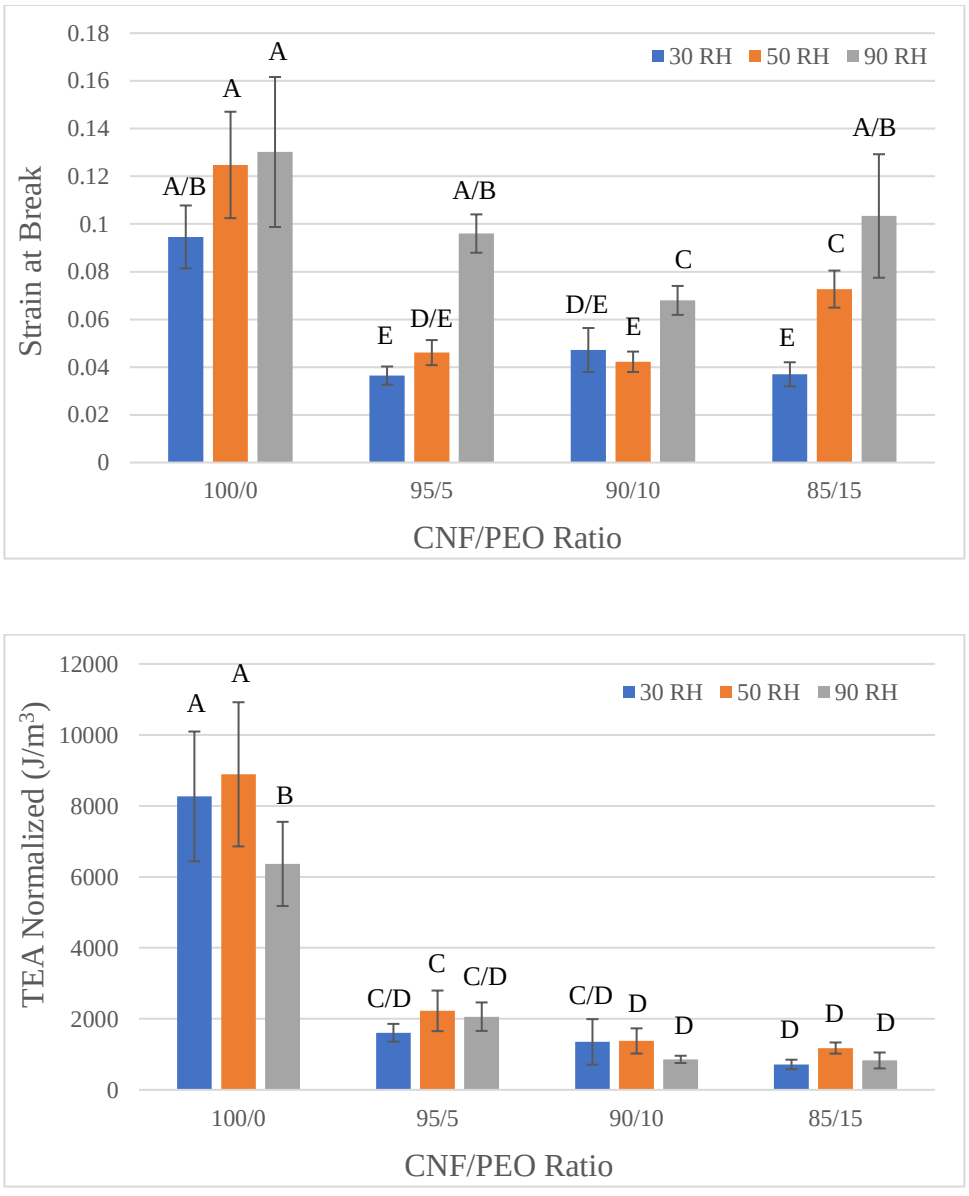

Figure 4.11. Strain at break and Tensile energy absorption of the CNF/PEO composite films at 30%, 50% and 90% RH.

4.2. Fourier-transform infrared spectroscopy with attenuated total reflection (FTIR-ATR)

The FTIR spectra of CNF/PEO composite films are shown in Figure 4.12. The absorption band at around 3300 cm^{-1} was observed for pure CNF and PEO films, attributed to the OH group.

In the 100% CNF film, this absorption band was 3313 $cm^{-1,}$ and the same band for PEO showed a peak at 3328 cm^{-1}. This indicates that with increasing PEO content, the hydrogen bond between PEO and CNF became stronger, which serves as a good barrier in terms of grease resistance (H. Tayeb et al. 2020). At 2900 cm^{-1}, the peak corresponds to C–H groups, and at approximately 1000 cm^{-1}, the peak corresponds to C–O groups (de Cuadro et al. 2015; Joly et al. 1999). These peaks correspond to the cellulose structure and this peak stretches higher with increasing PEO content.

The CNF/PEO composite film showed an increased wavenumber of 3334 cm^{-1} and 3336 cm^{-1} for the composite films with 17 and 30 wt.% of PEO, respectively. This absorption band further shifted to 3338 cm^{-1} for films with 41 wt.% PEO. The band shifting to a higher wavenumber is mainly caused by adding PEO to the CNF matrix. The shift of this band to a higher wavenumber was ascribed to the increased hydrogen bonding between CNF and PEO (Kondo and Sawatari 1994). The literature also reported that the intermolecular hydrogen bonds of cellulose molecules were replaced by the hydrogen bonds between PEO and CNF in the CNF/PEO films (Fukuya N et al. 2017).

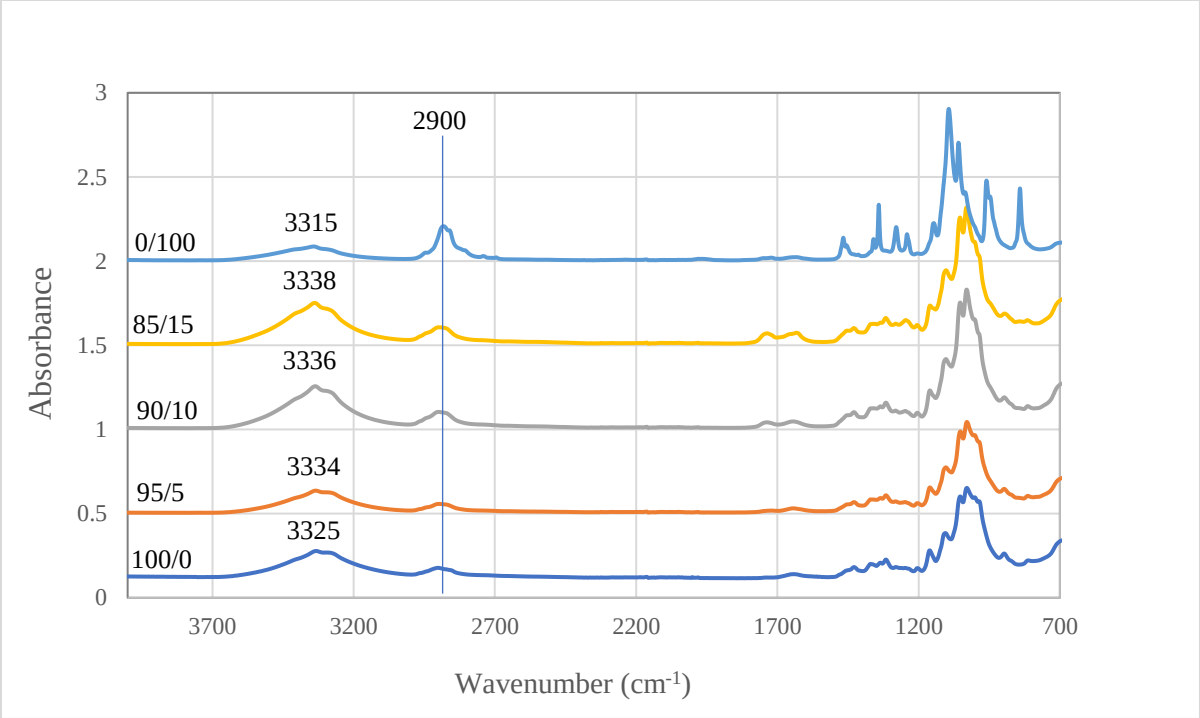

Figure 4.12. FTIR analysis of CNF/PEO composite films at a ratio of 100/0, 95/5, 90/10, 85/15 and 0/100

4.3. Atomic Force Microscopy (AFM)

The surface morphology of the CNF/CNC composite films with weight ratios of 100/0, 85/15, 70/30, 55/45, 30/70, and 0/100, are shown in Figure 4.13. It was observed that the 100% CNC film sample exhibited a short needle-like/rod-like structure and the particles were distributed evenly on the surface. In contrast, the 100% CNF film sample showed the distribution of fibrous network structure with larger pores, which showed in darker areas. The AFM micrographs confirm that 100% CNC film has low surface roughness, and the surface was smooth and compact in comparison to the 100% CNF film surface. The difference in contrasts in the images indicates different heights. Notably, the 100% CNF film is more porous than the 100% CNC film. As the CNC loading level increased in the CNF/CNC composite films, the porosity of the films decreased,

which helped to get a smoother surface. The average roughness values (expressed in Ra) for the 100% CNF and 100% CNC films were 40.14 ± 6.24 nm and 2.67 ± 0.36 nm, respectively.

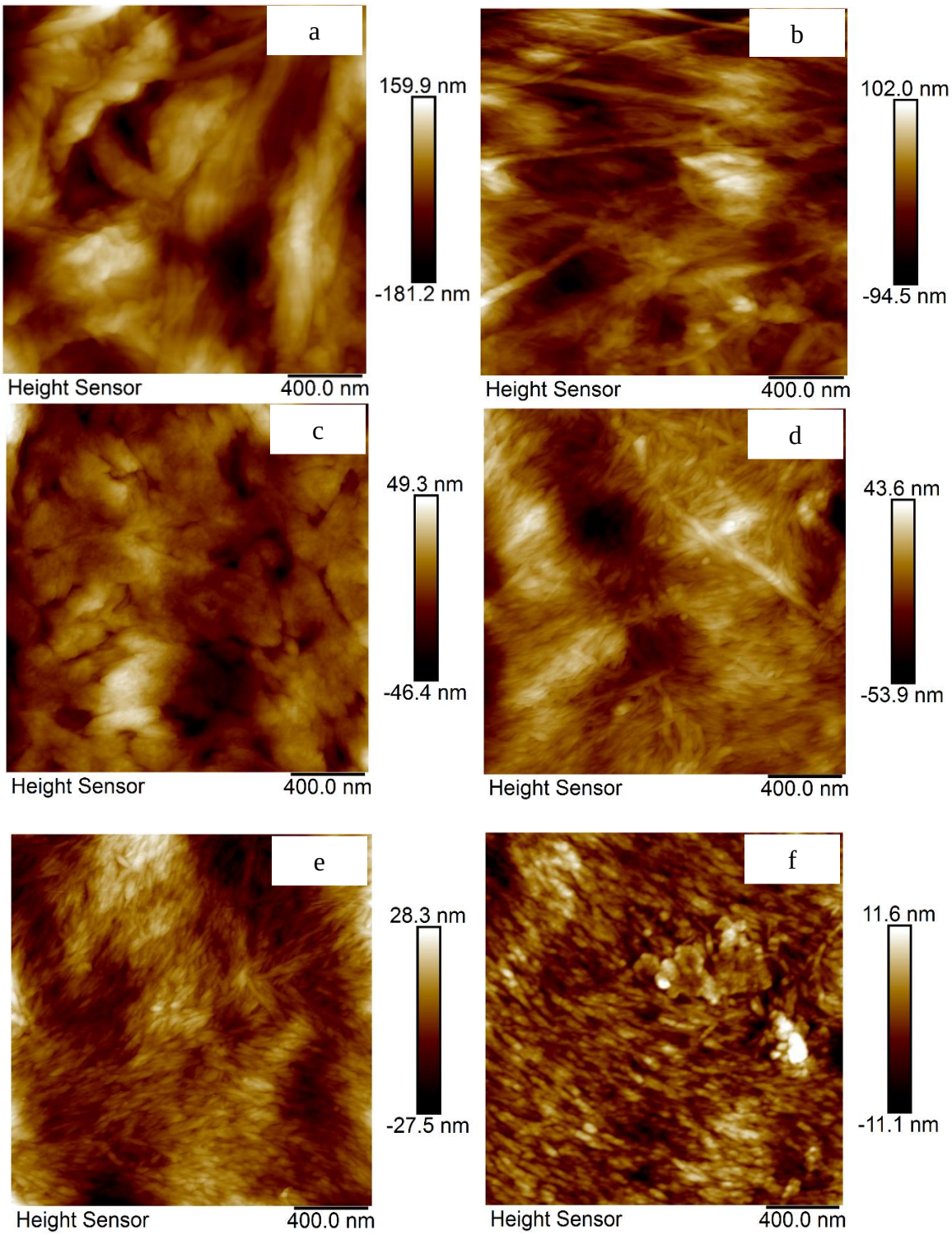

Figure 4.13. The AFM height diagrams of CNF/CNC composite films on sensors at weight ratios of 100/0 (a), 85/15 (b), 70/30 (c), 55/45 (d), 30/70 (e), and 0/100 (f).

The AFM height images of the CNF/PEO composite films with the PEO contents of 17, 30, and 41 wt.% and the pure PEO film are shown in Figure 4.14. The AFM images show that CNFs were arranged randomly (Figure 4.14. a). In the CNF/PEO composite film with 17 wt.%, PEO content, a large number of CNF bundles are visible (Figure 4.14. b). As the PEO ratio increased in the composite films, many small-diameter fibrils were observed (Figure 4.14. c). Likewise, the films become less porous as the PEO loading level increases. For the 100% PEO film (Figure 1.14 d), a flat surface with no fibers and no visible pores was observed. This indicates that the addition of PEO could seal the pores of CNF films resulting in a much smoother surface. In addition, from the AFM height images, it can be observed that as the PEO loading level increased, the agglomeration of CNF fibers decreased which helped get a smoother surface. Furthermore, as the PEO loading level increased, the larger pores showed darker color reduction, which is an advantageous feature of using PEO in CNF film formulation to block the pores and make the films/coating material grease resistant. Further study was conducted to analyze the pore size distribution of CNF/PEO composite films.

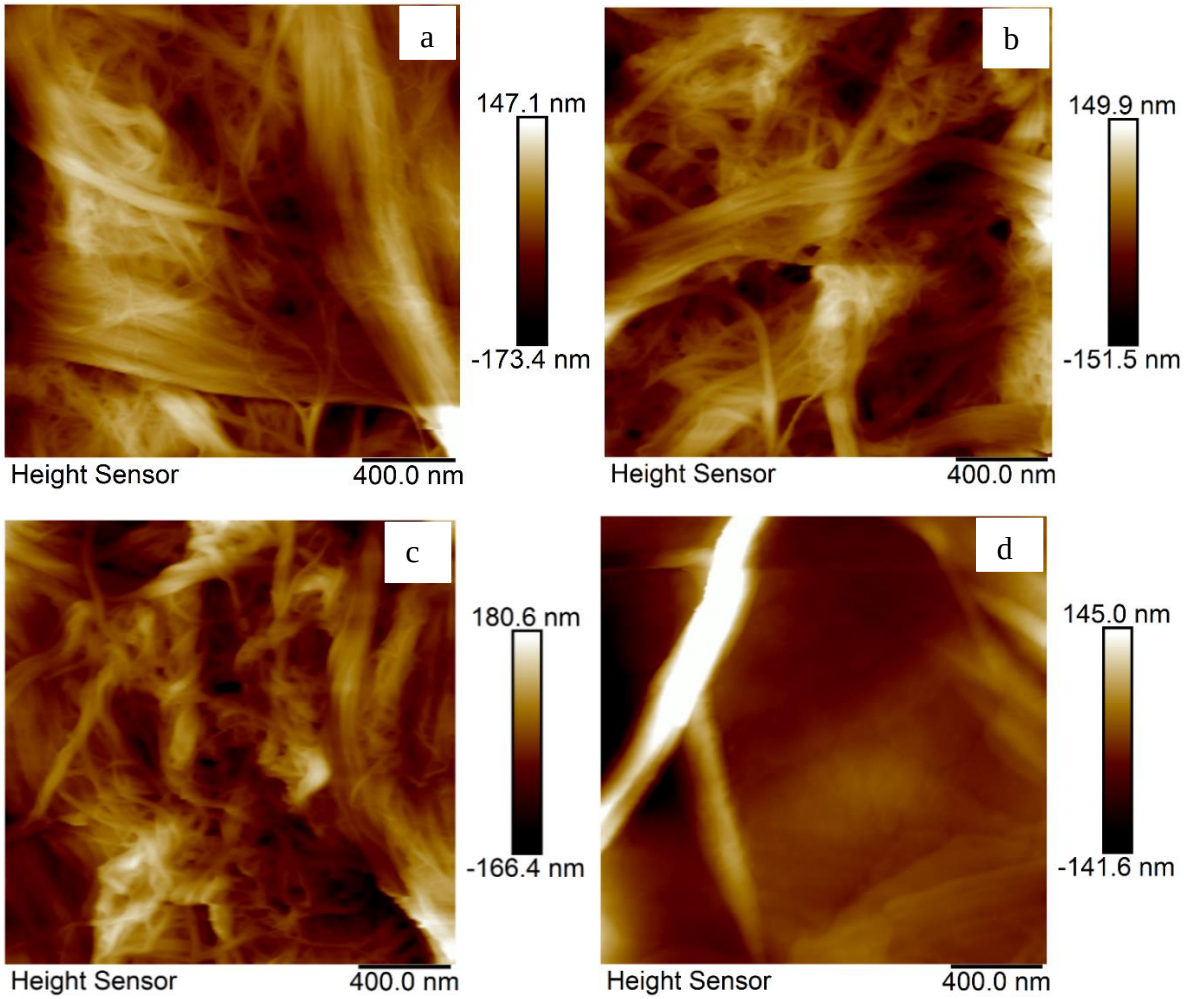

Figure 4.14. The AFM height diagrams of CNF/PEO composite films with the PEO content of 17 (a), 30 (b), and 41 wt.% (d) and the pure PEO film.

4.4. Pore size distribution

The pore size distributions of CNF/PEO composite films are shown in Figure 4.15. As the PEO loading level increased in the films, the proportion of the larger diameter of pores decreased. For instance, the film prepared at the highest loading level of PEO (41 wt.% PEO in the composite film) showed that most of the pores of the film were located between 0 to 1.75 microns, and the largest pore diameter is around 17 microns. The 100% CNF film showed a wide range of diameters

of pores up to 30 microns. The pore size distribution results indicate that PEO helped to reduce the pore size of CNF film.

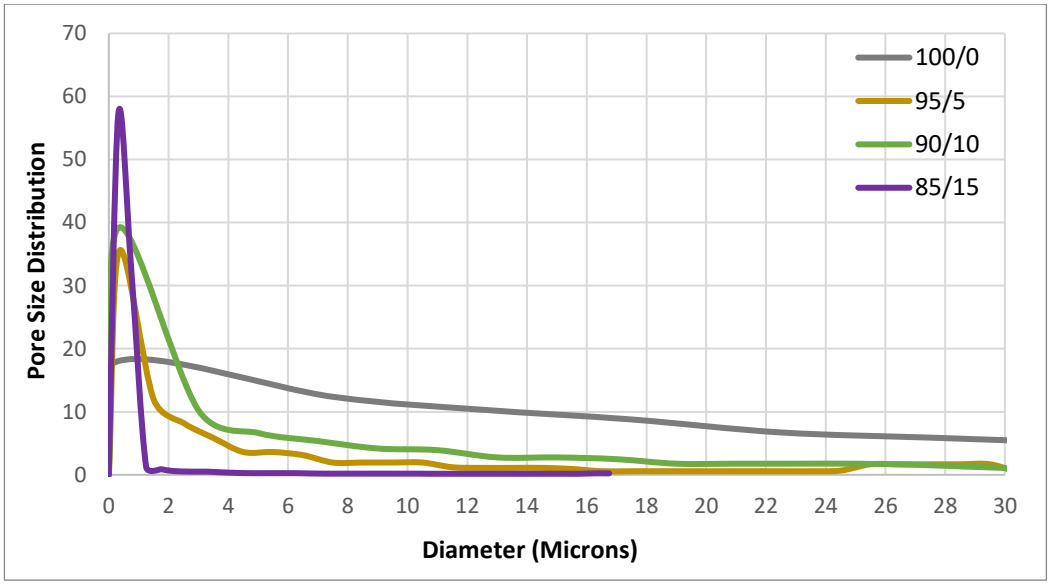

Figure 4.15. The pore size distributions of CNF/PEO composite films.

4.5. Contact angle measurement

The measured contact angles (CAs) of water as a function of time for the CNF/CNC composite films and commercial paper products are shown in Figure.4.16. Contact angles were counted from 0.5 min to 5 min. The CNF/CNC films and copy paper showed a much better surface wettability (i.e., smaller CAs) by water than other commercial paper products, namely parchment paper, pan liner, and butcher paper. At the beginning of the wetting process, the CAs for the 100% CNF films were 36.5° (±11.9) which decreased to 22.7° (±2.9) with an increasing period (5 min). However, as the CNC loading level increased in the films, the CAs decreased. For the 100% CNC film, the CA was 49.8° at 30 sec, then decreased to 41.2° at 5 min. It can be observed that with the

same period (5 min), the contact angle of water on the 100% CNF film surface decreased by 69 % while the water CA on the CNC film decreased by 20 %, which indicated that pure CNC film is more stable in contact with water than for pure CNF film.

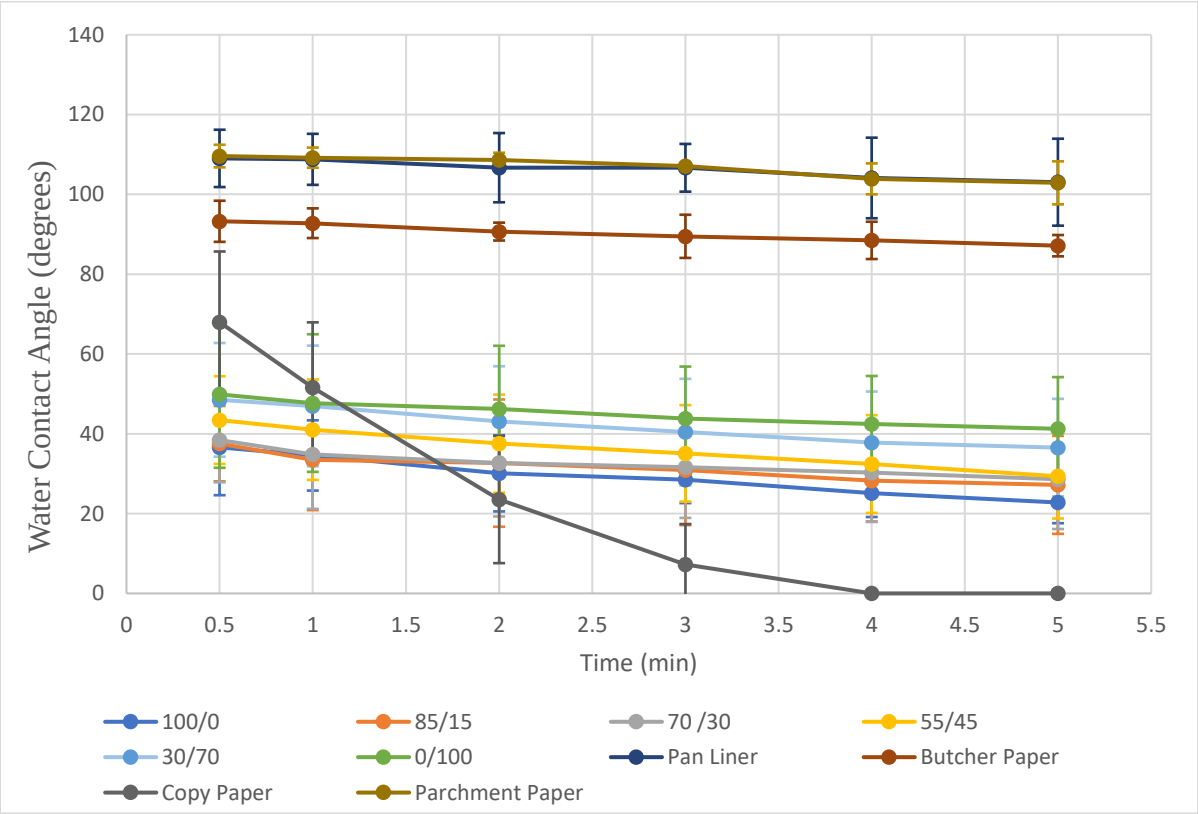

Figure 4.16. The contact angle data for water on CNF/CNC composite films and commercial paper products.

The reason behind such a phenomenon could be the chemical component of CNC. As we discussed earlier, CNC contains a higher degree of the crystalline region of cellulose, which is less sensitive to water than the amorphous region that can absorb water. Another possible reason could

be the porous structure of the CNF film, which accelerates the water to go through the pores and interact with the fibers, resulting in a rapid CAs decrease.

In contrast, adding the PEO in the CNF film formulation decreased the overall water contact angle with time shown in Figure 4.17. For instance, 100% CNF film showed a CA of 36.5° (±11.9) at 30 sec whereas the films prepared with the PEO content of 17, 30, and 41 wt. %, showed a much lower CAs of 5.6° (±0.5), 5.8° (±0.8) and 6.3° (±0.1), respectively at the same time frame. Furthermore, at five minutes, the 100% CNF showed a CA of 22.9° (±2.9) while the films prepared with the PEO content of 17, 30, and 41 wt. % showed much lower CAs of 3.5° (±1.1), 2.8° (±1.0) and 1.5° (±0.6), respectively. The reason behind such phenomena could be the reduced porosity of the CNF/PEO films, as shown in Figure 4.15. As the PEO content in the films increased, more pores were blocked, which might lead to a smoother surface and helped the spreading of water droplets faster resulting in lower contact angle. Another reason could be the higher moisture content in CNF/PEO composite film in comparison to pure CNF film, which was discussed earlier (Figure 4.8). Due to higher moisture content, films prepared with CNF/PEO might absorb water more rapidly in comparison to pure CNF film, resulting in lower contact angles.

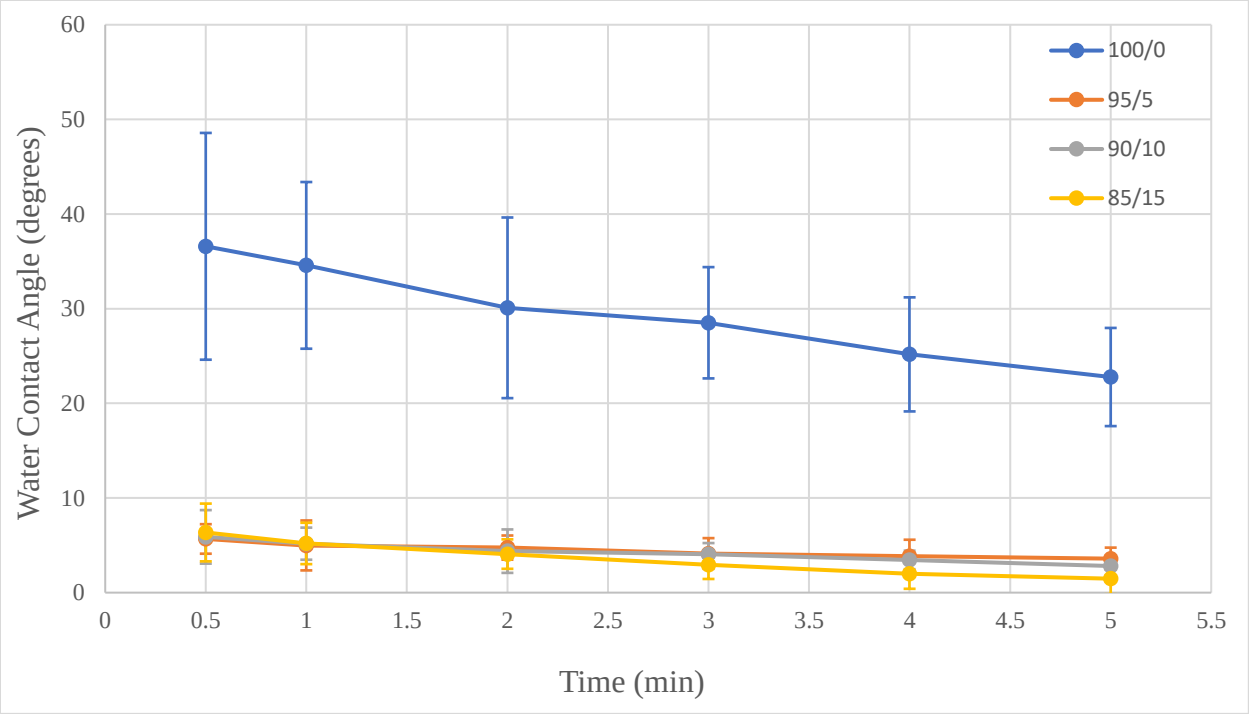

Figure 4.17. The water contact angle of the CNF/PEO composite films.

Another set of experiments was carried out to understand the effect of the film thickness on water CA. The effect of different thicknesses of the pure CNF and CNC films on water contact angles as a function of time is shown in Figures 4.18 and 4.19. The CNF films were prepared with the final thicknesses of 0.027 (± 0.03) mm, 0.037 (± 0.03) mm, 0.052 (± 0.02) mm, and 0.063 (± 0.03) mm. The water contact angle on the CNF film surface increased as the film thickness increased, which indicated that the CNF film showed less wettability with increasing film thickness. The CNF film at 0.063 mm thickness has a CA of 47.8° at 30 sec, which decreased to 28.1° at 5 min. Films prepared at 0.052 mm and 0.037 mm thickness showed similar CAs at 36.5° at 30 sec, then reduced to around 21.6°. However, the lowest thickness of the CNF film (0.027 mm) showed a decrease in CAs from 13.4° to 1.7°. The water can quickly penetrate through the

CNF film at 0.027 mm. On the other hand, the water CAs of pure CNC films prepared at 0.032 (± 0.01) mm, 0.043 (± 0.01) mm, 0.022 (± 0.02) mm, and 0.011 (±0.01) mm thicknesses did not change significantly as a function of time (Figure 4.19). Even with a much smaller thickness (the thinnest CNC film with a thickness of 0.011 mm) compared with the CNF film (0.027), the water contact angle of the pure CNC film only changed from 34.5° at 30 sec to 30.7° at 5 minutes.

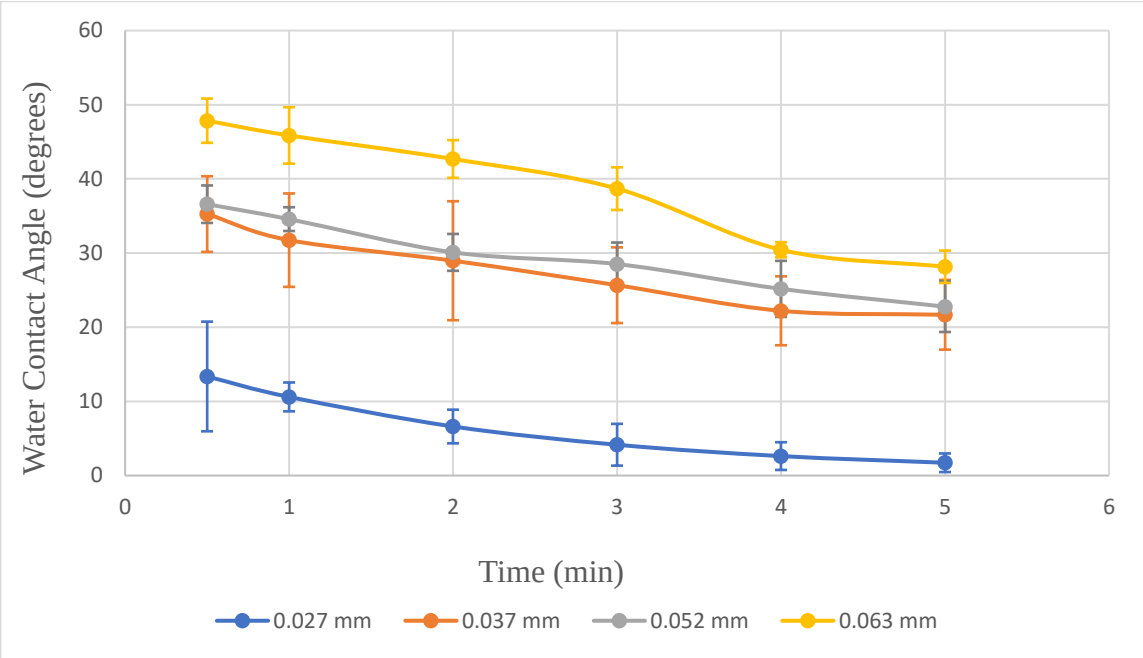

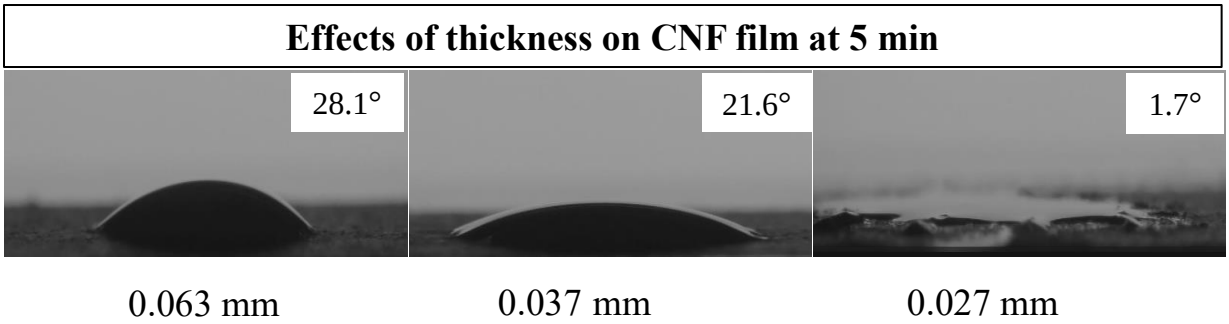

Figure 4.18. The effect of the CNF film thickness on water contact angle.

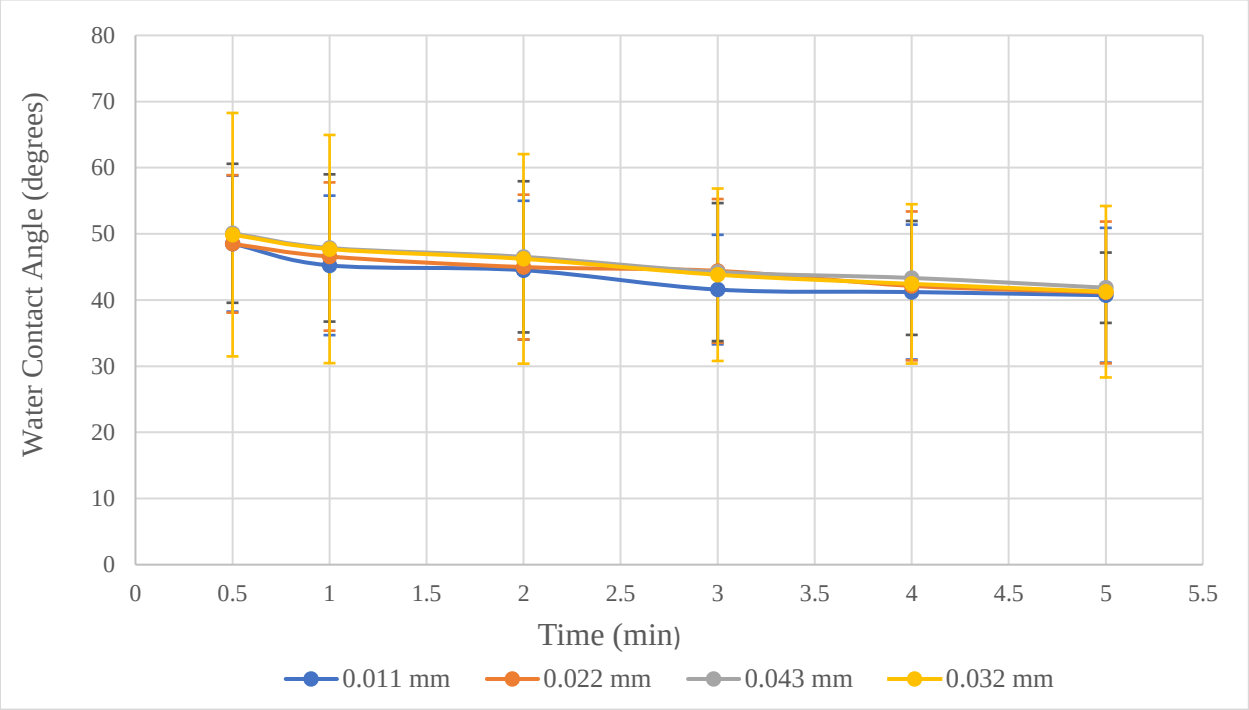

Figure 4.19. The effect of CNC film thickness on water contact angle.

4.7. Oil and grease resistance

Our major goal is to prepare oil and grease-resistant films for food packaging applications. Therefore, grease-resistant tests play an essential role. An example of a ‘‘pass” and “or fail” of a kit test is shown in Figure 4.22. Kit solution 12 was used in this experiment. All the prepared films, including CNF/CNC, CNF/PEO-based films, and films prepared at different thicknesses, showed a “pass” in kit test-12 by showing no dark surfaces after treating the paper with oil/solvents kit solution rating 12. It indicates that no penetration of oil occurred through prepared films. However, copy paper showed a “fail” test. A dark surface was observed after placing one drop of kit solution 12 on the surface of copy paper, thus indicating oil penetration through copy paper. However, all the other commercial paper products “pass” kit solution 12.

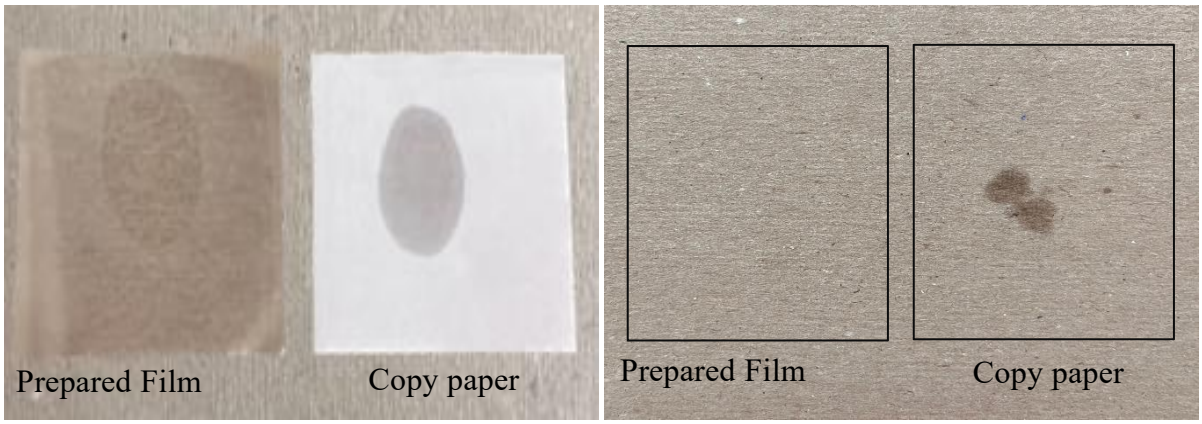

(a) **(b)**

Figure 4.20. Oil and grease resistance test : (a) before kit test (b) after kit test

5. Conclusions

This research analyzed the physical and mechanical properties of CNF/CNC-based films for grease resistance food packaging applications. The pure CNF film showed better tensile strength, strain at break, and tensile energy absorption compared to films loaded with the highest (70 wt%) CNC which showed better Young's modulus. However, the addition of different loading levels of PEO into CNF film formulation lowered mechanical properties except for strain at break value which showed an opposite trend. AFM images showed CNC film surface is smoother compared to CNF film and with the increasing addition of CNC loading level into CNF matrix, the film surface became smoother. As CNC can cause brittleness hence PEO has been added to the CNF matrix and films became more uniform and smooth with increasing PEO loading level. The water CAs of CNF films increased with increasing film thickness. In contrast, the CNC films at different thicknesses didn't show any significant change in CAs as a function of time. In terms of grease resistance, all CNF/CNC composite films and films prepared at different thicknesses passed the grease resistance test with a kit rating of 12. In addition, all the CNF/CNC composite films and CNF/PEO composite films passed the grease resistance test of 12 kit ratings. However, CNF/PEO composite film 85/15 ratio showed the lowest pore size distribution, which is a vital factor for grease resistance. With all the characterization techniques, CNF/PEO films at a ratio of 85/15 could be optimal for grease resistance food packaging applications.

6. Limitations and Future Recommendations

One of the main limitations of preparing such films is that, it requires seven days to dry in air which is time-consuming. Another limitation is that films prepared with CNF and PEO require high drying temperatures like 105 °C. Furthermore, the preparation of PEO solution at room temperature is also time-consuming. Therefore, some future recommendations have been suggested.

Firstly, oven drying temperature plays an important role in CNF/PEO film preparation. In addition, oven drying time holds another important parameter to fully dry CNF/PEO films. In this research work, we have used 105 °C oven drying temperature with 6 hr oven drying time. However, it is important to observe CNF/PEO film behavior at a slow drying process which means lower oven-drying temperature with prolonged oven-drying time.

Secondly, the preparation of PEO solution and the mixing temperature for the CNF suspension and PEO solution is an important parameter in preparing CNF/PEO composite films. In this research work, we used room temperature to mix CNF suspension and PEO solution. According to Li & Matsuba (2019), increasing mixing temperature can improve PEO chain mobility to form a more extensive deformation network and decrease the number of entanglements. Hence, in future work, we want to observe the effect of mixing temperature on the CNF/PEO film properties.

Finally, instead of preparing the standalone film, coating on paperboard using the optimum CNF/PEO ratio would be another recommendation for the future to understand the coating behavior of CNF/PEO formulation.

References

Aulin, C., Gällstedt, M., and Lindström, T. (2010). "Oxygen and oil barrier properties of microfibrillated cellulose films and coatings," *Cellulose*, 17(3), 559–574. DOI: 10.1007/s10570-009-9393-y

Azeredo, H. M. C., Rosa, M. F., and Mattoso, L. H. C. (2017). "Nanocellulose in bio-based food packaging applications," *Industrial Crops and Products*, 97, 664–671. DOI: 10.1016/j.indcrop.2016.03.013

Bajpai, P. (2012). "Brief Description of the Pulp and Paper Making Process," in: *Biotechnology for Pulp and Paper Processing*, Springer US, Boston, MA, 7–14. DOI: 10.1007/978-1-4614-1409-4_2

Baran, J. R. (2001). "Fluorinated Surfactants and Repellents: Second Edition, Revised and Expanded Surfactant Science Series. Volume 97. By Erik Kissa (Consultant, Wilmington, DE). Marcel Dekker: New York. 2001. xiv + 616 pp. $195.00. ISBN 0-8247-0472-X.," *Journal of the American Chemical Society*, 123(36), 8882–8882. DOI: 10.1021/ja015260a

Bardet, R., Reverdy, C., Belgacem, N., Leirset, I., Syverud, K., Bardet, M., and Bras, J. (2015). "Substitution of nanoclay in high gas barrier films of cellulose nanofibrils with cellulose nanocrystals and thermal treatment," *Cellulose*, 22(2), 1227–1241. DOI: 10.1007/s10570-015-0547-9

Begley, T. H., Hsu, W., Noonan, G., and Diachenko, G. (2008). "Migration of fluorochemical paper additives from food-contact paper into foods and food simulants," *Food Additives & Contaminants: Part A*, 25(3), 384–390. DOI: 10.1080/02652030701513784

Benítez, A. J., Torres-Rendon, J., Poutanen, M., and Walther, A. (2013). "Humidity and Multiscale Structure Govern Mechanical Properties and Deformation Modes in Films of Native Cellulose Nanofibrils," *Biomacromolecules*, 14(12), 4497–4506. DOI: 10.1021/bm401451m

Biermann, C. J. (1996). "Paper manufacture," in: *Handbook of Pulping and Papermaking*, Academic Press, San Diego, CA, 209.

Birnbaum, L. S., and Grandjean, P. (2015). "Alternatives to PFASs: Perspectives on the Science," *Environmental Health Perspectives*, 123(5). DOI: 10.1289/ehp.1509944

Blum, A., Balan, S. A., Scheringer, M., Trier, X., Goldenman, G., Cousins, I. T., Diamond, M., Fletcher, T., Higgins, C., Lindeman, A. E., Peaslee, G., de Voogt, P., Wang, Z., and Weber, R. (2015). "The Madrid Statement on Poly- and Perfluoroalkyl Substances (PFASs)," *Environmental Health Perspectives*, 123(5). DOI: 10.1289/ehp.1509934

Chen, C., and Hu, L. (2018). “Nanocellulose toward Advanced Energy Storage Devices: Structure and Electrochemistry,” *Accounts of Chemical Research*, 51(12), 3154–3165. DOI: 10.1021/acs.accounts.8b00391

Chen, C., Liu, W., Wang, Z., Peng, K., Pan, W., and Xie, Q. (2015). “Novel form stable phase change materials based on the composites of polyethylene glycol/polymeric solid-solid phase change material,” *Solar Energy Materials and Solar Cells*, 134, 80–88. DOI: 10.1016/j.solmat.2014.11.039

Chen, W., Yu, H., Lee, S.-Y., Wei, T., Li, J., and Fan, Z. (2018). “Nanocellulose: a promising nanomaterial for advanced electrochemical energy storage,” *Chemical Society Reviews*, 47(8), 2837–2872. DOI: 10.1039/C7CS00790F

Choi, Y., and Simonsen, J. (2006). “Cellulose Nanocrystal-Filled Carboxymethyl Cellulose Nanocomposites,” *Journal of Nanoscience and Nanotechnology*, 6(3), 633–639. DOI: 10.1166/jnn.2006.132

de Cuadro, P., Belt, T., Kontturi, K. S., Reza, M., Kontturi, E., Vuorinen, T., and Hughes, M. (2015). “Cross-linking of cellulose and poly(ethylene glycol) with citric acid,” *Reactive and Functional Polymers*, 90, 21–24. DOI: 10.1016/j.reactfunctpolym.2015.03.007

Deshwal, G. K., Panjagari, N. R., and Alam, T. (2019a). “An overview of paper and paper based food packaging materials: health safety and environmental concerns,” *Journal of Food Science and Technology*, 56(10), 4391–4403. DOI: 10.1007/s13197-019-03950-z

Deshwal, G. K., Panjagari, N. R., and Alam, T. (2019b). “An overview of paper and paper based food packaging materials: health safety and environmental concerns,” *Journal of Food Science and Technology*, 56(10), 4391–4403. DOI: 10.1007/s13197-019-03950-z

Fallahi, A., Guldentops, G., Tao, M., Granados-Focil, S., and van Dessel, S. (2017). “Review on solid-solid phase change materials for thermal energy storage: Molecular structure and thermal properties,” *Applied Thermal Engineering*, 127, 1427–1441. DOI: 10.1016/j.applthermaleng.2017.08.161

Fernández-Santos, J., Valls, C., Cusola, O., and Roncero, M. B. (2022). “Composites of cellulose nanocrystals in combination with either cellulose nanofibril or carboxymethylcellulose as functional packaging films,” *International Journal of Biological Macromolecules*, 211, 218–229. DOI: 10.1016/j.ijbiomac.2022.05.049

Ferrer, A., Pal, L., and Hubbe, M. (2017). “Nanocellulose in packaging: Advances in barrier layer technologies,” *Industrial Crops and Products*, 95, 574–582. DOI: 10.1016/j.indcrop.2016.11.012

Fischer, D. (2020). “The effect of molecular weight and deposition temperature on the formation of poly(ethylene oxide) films using the femtosecond pulsed laser deposition,” *POLYMER CRYSTALLIZATION*, 3(5). DOI: 10.1002/pcr2.10153

Geyer, R., Jambeck, J. R., and Law, K. L. (2017). "Production, use, and fate of all plastics ever made," *Science Advances*, 3(7). DOI: 10.1126/sciadv.1700782

H. Tayeb, A., Tajvidi, M., and Bousfield, D. (2020). "Paper-Based Oil Barrier Packaging using Lignin-Containing Cellulose Nanofibrils," *Molecules*, 25(6), 1344. DOI: 10.3390/molecules25061344

Harris, M. J. (2013). *Poly(Ethylene Glycol) Chemistry: Biotechnical and Biomedical Applications*, Springer.

Henriksson, M., Berglund, L. A., Isaksson, P., Lindström, T., and Nishino, T. (2008). "Cellulose Nanopaper Structures of High Toughness," *Biomacromolecules*, 9(6), 1579–1585. DOI: 10.1021/bm800038n

Hubbe, M. A., Ferrer, A., Tyagi, P., Yin, Y., Salas, C., Pal, L., and Rojas, O. J. (2017). "Nanocellulose in Thin Films, Coatings, and Plies for Packaging Applications: A Review," *BioResources*, 12(1), 2143–2233. DOI: 10.15376/biores.12.1.2143-2233

J. Huang, X. Ma, G. Yang, A. D. (n.d.). "'Introduction to Nanocellulose'. In J. Huang, A. Dufresne N. Lin. Nanocellulose: From Fundamentals to Advanced Materials, Weinheim, Willey-VCH Verlag GmbH & Co. LGaA, 2019, pp. 1-15."

Jang, E.-S., and Kang, C.-W. (2020). "Do Face Masks become Worthless after Only One Use in the COVID-19 Pandemic?," *Infection & Chemotherapy*, 52(4), 583. DOI: 10.3947/ic.2020.52.4.583

Javed, A., Ullsten, H., and Järnström, L. (2017). "Effects on Oxygen-barrier Properties of Pretreating Paperboard with a Starch-Poly(Vinyl Alcohol) Blend before Polyethylene Extrusion," *Packaging Technology and Science*, 30(8), 399–410. DOI: 10.1002/pts.2210

Joly, C., Le Cerf, D., Chappey, C., Langevin, D., and Muller, G. (1999). "Residual solvent effect on the permeation properties of fluorinated polyimide films," *Separation and Purification Technology*, 16(1), 47–54. DOI: 10.1016/S1383-5866(98)00118-X

Khwaldia, K., Arab-Tehrany, E., and Desobry, S. (2010). "Biopolymer Coatings on Paper Packaging Materials," *Comprehensive Reviews in Food Science and Food Safety*, John Wiley & Sons, Ltd, 9(1), 82–91. DOI: 10.1111/J.1541-4337.2009.00095.X

Kisonen, V., Prakobna, K., Xu, C., Salminen, A., Mikkonen, K. S., Valtakari, D., Eklund, P., Seppälä, J., Tenkanen, M., and Willför, S. (2015). "Composite films of nanofibrillated cellulose and O-acetyl galactoglucomannan (GGM) coated with succinic esters of GGM showing potential as barrier material in food packaging," *Journal of Materials Science*, 50(8), 3189–3199. DOI: 10.1007/s10853-015-8882-7

Kjellgren, H., Gällstedt, M., Engström, G., and Järnström, L. (2006). "Barrier and surface properties of chitosan-coated greaseproof paper," *Carbohydrate Polymers*, 65(4), 453–460. DOI: 10.1016/j.carbpol.2006.02.005

Kondo, T., and Sawatari, C. (1994). “Intermolecular hydrogen bonding in cellulose/poly(ethylene oxide) blends: thermodynamic examination using 2,3-di-O- and 6-O-methylcelluloses as cellulose model compounds,” *Polymer*, 35(20), 4423–4428. DOI: 10.1016/0032-3861(94)90102-3

Krafft, M. P., and Riess, J. G. (2015). “Selected physicochemical aspects of poly- and perfluoroalkylated substances relevant to performance, environment and sustainability—Part one,” *Chemosphere*, 129, 4–19. DOI: 10.1016/j.chemosphere.2014.08.039

Kumar, V., Bollström, R., Yang, A., Chen, Q., Chen, G., Salminen, P., Bousfield, D., and Toivakka, M. (2014). “Comparison of nano- and microfibrillated cellulose films,” *Cellulose*, 21(5), 3443–3456. DOI: 10.1007/s10570-014-0357-5

Leppänen, I., Hokkanen, A., Österberg, M., Vähä-Nissi, M., Harlin, A., and Orelma, H. (2022). “Hybrid films from cellulose nanomaterials—properties and defined optical patterns,” *Cellulose*, 29(16), 8551–8567. DOI: 10.1007/s10570-022-04795-0

Li, Y., Wu, M., Liu, R., and Huang, Y. (2009). “Cellulose-based solid–solid phase change materials synthesized in ionic liquid,” *Solar Energy Materials and Solar Cells*, 93(8), 1321–1328. DOI: 10.1016/j.solmat.2009.02.005

Liang, X.-H., Guo, Y.-Q., Gu, L.-Z., and Ding, E.-Y. (1995). “Crystalline-Amorphous Phase Transition of Poly(ethylene Glycol)/Cellulose Blend,” *Macromolecules*, 28(19), 6551–6555. DOI: 10.1021/ma00123a023

Mayer, F. F. (1860). “Technical intelligence—Vegetable parchment—Papyrene,” *The American Journal of Science and Arts*, 86(29), 278.

Meng, Q., and Wang, T. J. (2019). “Mechanics of Strong and Tough Cellulose Nanopaper,” *Applied Mechanics Reviews*, 71(4). DOI: 10.1115/1.4044018

Miettinen, A., Chinga-Carrasco, G., and Kataja, M. (2014). “Three-Dimensional Microstructural Properties of Nanofibrillated Cellulose Films,” *International Journal of Molecular Sciences*, 15(4), 6423–6440. DOI: 10.3390/ijms15046423

Mo, J., Zhang, D., Sun, M., Liu, L., Hu, W., Jiang, B., Chu, L., and Li, M. (2021). “Polyethylene Oxide as a Multifunctional Binder for High-Performance Ternary Layered Cathodes,” *Polymers*, 13(22), 3992. DOI: 10.3390/polym13223992

Moon, R. J., Martini, A., Nairn, J., Simonsen, J., and Youngblood, J. (2011). “Cellulose nanomaterials review: structure, properties and nanocomposites,” *Chemical Society Reviews*, 40(7), 3941. DOI: 10.1039/c0cs00108b

Mudumbi, J. B. N., Ntwampe, S. K. O., Matsha, T., Mekuto, L., and Itoba-Tombo, E. F. (2017). “Recent developments in polyfluoroalkyl compounds research: a focus on human/environmental health impact, suggested substitutes and removal strategies,”

Environmental Monitoring and Assessment, 189(8), 402. DOI: 10.1007/s10661-017-6084-2

Nair, S. S., Zhu, J., Deng, Y., and Ragauskas, A. J. (2014). "High performance green barriers based on nanocellulose," *Sustainable Chemical Processes*, 2(1), 23. DOI: 10.1186/s40508-014-0023-0

Nechyporchuk, O., Belgacem, M. N., and Bras, J. (2016). "Production of cellulose nanofibrils: A review of recent advances," *Industrial Crops and Products*, 93, 2–25. DOI: 10.1016/j.indcrop.2016.02.016

Omran, A. A. B., Mohammed, A. A. B. A., Sapuan, S. M., Ilyas, R. A., Asyraf, M. R. M., Rahimian Koloor, S. S., and Petrů, M. (2021). "Micro- and Nanocellulose in Polymer Composite Materials: A Review," *Polymers*, 13(2), 231. DOI: 10.3390/polym13020231

Österberg, M., Vartiainen, J., Lucenius, J., Hippi, U., Seppälä, J., Serimaa, R., and Laine, J. (2013). "A Fast Method to Produce Strong NFC Films as a Platform for Barrier and Functional Materials," *ACS Applied Materials & Interfaces*, 5(11), 4640–4647. DOI: 10.1021/am401046x

Peng, K., Chen, C., Pan, W., Liu, W., Wang, Z., and Zhu, L. (2016). "Preparation and properties of β-cyclodextrin/4,4′-diphenylmethane diisocyanate/polyethylene glycol (β-CD/MDI/PEG) crosslinking copolymers as polymeric solid–solid phase change materials," *Solar Energy Materials and Solar Cells*, 145, 238–247. DOI: 10.1016/j.solmat.2015.10.031

Phuong, H. T., Thoa, N. K., Tuyet, P. T. A., Van, Q. N., and Hai, Y. D. (2022). "Cellulose Nanomaterials as a Future, Sustainable and Renewable Material," *Crystals*, 12(1), 106. DOI: 10.3390/cryst12010106

Ramírez Carnero, A., Lestido-Cardama, A., Vazquez Loureiro, P., Barbosa-Pereira, L., Rodríguez Bernaldo de Quirós, A., and Sendón, R. (2021). "Presence of Perfluoroalkyl and Polyfluoroalkyl Substances (PFAS) in Food Contact Materials (FCM) and Its Migration to Food," *Foods*, 10(7), 1443. DOI: 10.3390/foods10071443

Roman, M., Haring, A. P., and Bertucio, T. J. (2019). "The growing merits and dwindling limitations of bacterial cellulose-based tissue engineering scaffolds," *Current Opinion in Chemical Engineering*, 24, 98–106. DOI: 10.1016/j.coche.2019.03.006

Schaider, L. A., Balan, S. A., Blum, A., Andrews, D. Q., Strynar, M. J., Dickinson, M. E., Lunderberg, D. M., Lang, J. R., and Peaslee, G. F. (2017). "Fluorinated Compounds in U.S. Fast Food Packaging," *Environmental Science & Technology Letters*, 4(3), 105–111. DOI: 10.1021/acs.estlett.6b00435

Shi, Z., Xu, H., Yang, Q., Xiong, C., Zhao, M., Kobayashi, K., Saito, T., and Isogai, A. (2019). "Carboxylated nanocellulose/poly(ethylene oxide) composite films as solid–

solid phase-change materials for thermal energy storage," *Carbohydrate Polymers*, 225, 115215. DOI: 10.1016/j.carbpol.2019.115215

Shojaeiarani, J., Bajwa, D. S., and Chanda, S. (2021). "Cellulose nanocrystal based composites: A review," *Composites Part C: Open Access*, 5, 100164. DOI: 10.1016/j.jcomc.2021.100164

Sirviö, J. A., Kolehmainen, A., Liimatainen, H., Niinimäki, J., and Hormi, O. E. O. (2014). "Biocomposite cellulose-alginate films: Promising packaging materials," *Food Chemistry*, 151, 343–351. DOI: 10.1016/j.foodchem.2013.11.037

Smook, G. A. (1992). "Overview of pulping methodology," in: *Handbook for Pulp & Paper Technologists*, Angus Wilde Publications, VC, BC, 36.

Thomas, B., Raj, M. C., B, A. K., H, R. M., Joy, J., Moores, A., Drisko, G. L., and Sanchez, C. (2018). "Nanocellulose, a Versatile Green Platform: From Biosources to Materials and Their Applications," *Chemical Reviews*, 118(24), 11575–11625. DOI: 10.1021/acs.chemrev.7b00627

Tyagi, P., Hubbe, M. A., Lucia, L., and Pal, L. (2018). "High performance nanocellulose-based composite coatings for oil and grease resistance," *Cellulose*, 25(6), 3377–3391. DOI: 10.1007/s10570-018-1810-7

Tyagi, P., Lucia, L. A., Hubbe, M. A., and Pal, L. (2019). "Nanocellulose-based multilayer barrier coatings for gas, oil, and grease resistance," *Carbohydrate Polymers*, 206, 281–288. DOI: 10.1016/j.carbpol.2018.10.114

Umair, M., Azis, N., Halis, R., and Jasni, J. (2020). "Investigation of Kenaf Paper in the Presence of PVA for Transformers Application," *Materials*, 13(21), 5002. DOI: 10.3390/ma13215002

Vanza, J. D., Patel, R. B., Dave, R. R., and Patel, M. R. (2020). "Polyethylene oxide and its controlled release properties in hydrophilic matrix tablets for oral administration," *Pharmaceutical Development and Technology*, 25(10), 1169–1187. DOI: 10.1080/10837450.2020.1808015

Vergara-Figueroa, J., Erazo, O., Pesenti, H., Valenzuela, P., Fernández-Pérez, A., and Gacitúa, W. (2022). "Development of Thin Films from Thermomechanical Pulp Nanofibers of Radiata Pine (Pinus radiata D. Don) for Applications in Bio-Based Nanocomposites," *Fibers*, 11(1), 1. DOI: 10.3390/fib11010001

Wang, L., Chen, C., Wang, J., Gardner, D. J., and Tajvidi, M. (2020). "Cellulose nanofibrils versus cellulose nanocrystals: Comparison of performance in flexible multilayer films for packaging applications," *Food Packaging and Shelf Life*, 23, 100464. DOI: 10.1016/j.fpsl.2020.100464

Wang, S., Li, T., Chen, C., Kong, W., Zhu, S., Dai, J., Diaz, A. J., Hitz, E., Solares, S. D., Li, T., and Hu, L. (2018). "Transparent, Anisotropic Biofilm with Aligned Bacterial

Cellulose Nanofibers," *Advanced Functional Materials*, 28(24), 1707491. DOI: 10.1002/adfm.201707491

Zhou, C., Chu, R., Wu, R., and Wu, Q. (2011). "Electrospun Polyethylene Oxide/Cellulose Nanocrystal Composite Nanofibrous Mats with Homogeneous and Heterogeneous Microstructures," *Biomacromolecules*, 12(7), 2617–2625. DOI: 10.1021/bm200401p